Origin and duration of late orogenic magmatism in the foreland of the Variscan belt (Lesponne - Chiroulet - Neouvielle area, french Pyrenees)

Baptiste Lemirre, Bryan Cochelin, Stéphanie Duchêne, Michel de Saint Blanquat, Marc Poujol

Accepted Manuscript

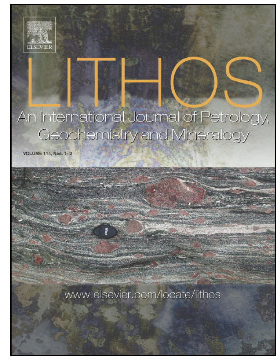

Origin and duration of late orogenic magmatism in the foreland of the Variscan belt (Lesponne — Chiroulet — Neouvielle area, french Pyrenees)

Baptiste Lemirre, Bryan Cochelin, Stéphanie Duchene, Michel de Saint Blanquat, Marc Poujol

PII: S0024-4937(19)30145-8
DOI: https://doi.org/10.1016/j.lithos.2019.03.037
Reference: LITHOS 5031

To appear in: *LITHOS*

Received date: 20 July 2018
Accepted date: 31 March 2019

Please cite this article as: B. Lemirre, B. Cochelin, S. Duchene, et al., Origin and duration of late orogenic magmatism in the foreland of the Variscan belt (Lesponne — Chiroulet — Neouvielle area, french Pyrenees), LITHOS, https://doi.org/10.1016/j.lithos.2019.03.037

Origin and duration of late orogenic magmatism in the foreland of the Variscan belt (Lesponne — Chiroulet — Neouvielle area, french Pyrenees)

Baptiste Lemirre[a,*], Bryan Cochelin[a,b,c], Stéphanie Duchene[a], Michel de Saint Blanquat[a], Marc Poujol[d]

[a]Géosciences Environnement Toulouse, Université de Toulouse, CNES, CNRS, IRD, UPS, Toulouse, France

[b]BRGM DGR/GSO, BP 36009, 45060 Orléans, France

[c]Univ. Orléans, CNRS, BRGM, ISTO – UMR 7327, F-45071 Orléans, France

[d]Univ. Rennes, CNRS, Géosciences Rennes – UMR 6118, F-35000 Rennes, France

[*]Corresponding author.

Abstract

During the late stage of the Variscan orogeny, the pyrenean segment underwent intense magmatism and regional high temperature – low pressure metamorphism. In the Lesponne – Chiroulet – Neouvielle area, a granodioritic pluton was emplaced in the upper crust while dioritic to granitic magmas were emplaced in metamorphic domes. Magmatism was contemporaneous with the regional crustal partial melting recorded in the core of the domes. The area is therefore a key target in the Pyrenees to discuss potential magmatic sources as well as the age and duration of the late Variscan magmatism. Geochemical data on representative magmatic rocks highlight two distinct sources of magma: a mantle source and a metasedimentary crustal source that produced respectively metaluminous and peraluminous magmas. Geochronological results show that magmatism took place over a period of about 10 My from ca. 303 to ca. 290 Ma. During this period, the middle to lower crust was composed of partially molten metasediments intruded by mantle and crustal magmas that crystallized in a final pulse at ca. 290 Ma. Late Variscan metamorphism and magmatism recorded in the Pyrenees have to be related to a significant and rapid heating from the underlying mantle rather than to crustal processes such as the maturation of a thickened continental crust. We propose that the initiation of metamorphism and bimodal magmatism at ca. 305 Ma in the Pyrenees is the expression of the delamination of the Gondwanan lithospheric mantle at a global scale in the Variscan belt.

Keywords: Variscan belt, Pyrenees, granitoid petrogenesis, U-Pb geochronology, HT-LP metamorphism

1. Introduction

Late stages of orogenic cycles are mostly characterized by abundant magmatism associated with high temperature – low pressure (HT–LP) metamorphism (Bonin, 2004; Vanderhaeghe, 2012). The origin of magmas and the duration of magmatism are therefore critical parameters for the understanding of the geodynamical context of late orogenic stages. Late orogenic evolution is well expressed in the Variscan orogeny, which ended by a widespread magmatism and a HT-LP metamorphism occurring throughout the belt (*e.g.* Henk et al., 2000; O'Brien, 2000). The Pyrenean segment of the belt is characterized by a diversified late Carboniferous to early Permian magmatism (mafic to felsic; peraluminous and metaluminous; calc-alkaline to alkaline magmas), synchronous with HT–LP metamorphism and with a major deformation event (Carreras and Debat, 1996; Debon et al., 1996; Guitard et al., 1996; Olivier et al., 2008; Aguilar et al., 2014; Denèle et al., 2014; Pereira et al., 2014; Cochelin et al., 2017). While moderate crustal thickening has been recognized in the Pyrenees (Azambre and Guitard, 2001), there is no evidence for a HP-LT metamorphism indicative of the Devonian subduction phase documented elsewhere in the Variscan realm (figure 1a, Matte, 1991, 2001). The presence of Carboniferous flysh deposits (Delvolve, 1996) further suggests that the Pyrenees constituted part of the southern foreland of the Variscan belt before the late HT-LP orogenic stage (Franke et al., 2011; Denèle et al., 2014; Franke, 2014; Cochelin et al., 2017). It is therefore of prime importance to study and understand the origin and the establishment of the late Variscan HT-LP thermal regime. Up to now, only few geochronological constraints are available on migmatites, anatectic granites and mafic to intermediate magmatic bodies in the Pyrenees. Recent works suggest that magmatic activity lasted until the middle Permian (Aguilar et al., 2014; Esteban et al., 2015; Kilzi et al., 2016). We present new geochronological data on migmatites and magmatic rocks from the Lesponne and Chiroulet gneiss domes and the Neouvielle pluton, in the western Axial Zone (figure 1b). These results are interpreted together with isotopic analysis and temperature estimates of the surrounding crustal metamorphic rocks in order to propose a chronology for the late Variscan evolution in the Pyrenees and to discuss the relative contribution of the mantle and crustal sources for the generation of the magmas as well as at the heat sources responsible for the HT-LP metamorphism.

2. Geological setting

The Variscan belt is an Upper Paleozoic orogeny resulting from the convergence between the Gondwana and Laurentia continents and the Avalonia and Armorica microcontinents (*e.g.* Matte, 1991, 2001; Martínez Catalán, 2011). The succession of subduction and collision led to high pressure – low temperature metamorphism during Devonian (Pin and Vielzeuf, 1983; Bosse et al., 2000; Roger and Matte, 2005; Giacomini et al., 2006; Paquette et al., 2017; Lotout et al., 2018). Then, the Variscan orogeny ended by a late high temperature event during Carboniferous to early Permian which led to widespread partial melting and magmatism throughout the belt (*e.g.* Burg et al., 1994; Gutiérrez-Alonso et al., 2011; Lardeaux, 2014; Schulmann et al., 2014; Gapais et al., 2015; Ballouard et al., 2015, 2017; Laurent et al., 2017; Poujol et al., 2017).

The Pyrenean segment of the Variscan belt is mainly composed of Precambrian to Permian sediments (Padel et al., 2018) affected by the late HT-LP event responsible for the emplacement of several gneiss domes and intruded by plutons between 310 Ma and 295 Ma under transpressional settings (Debon et al., 1996; Guitard et al., 1996; Roberts et al., 2000; Mezger et al., 2004; Mezger and Wissenschaften, 2005; Olivier et al., 2008; Aguilar et al., 2014; Denèle et al., 2014; Pereira et al., 2014; Cochelin et al., 2017; 2018). Gneiss domes are longitudinally elongated and were emplaced within the upper crust by horizontal E-W flow of the mid-lower crust at peak metamorphism (e.g. Denèle et al., 2014; Cochelin et al., 2017). The studied area is located in the western Axial Zone of the Pyrenees (figure 1b) where the great diversity of metamorphic and magmatic rocks is well exposed within the Lesponne and Chiroulet metamorphic domes and the Neouvielle pluton. The Lesponne and Chiroulet magmatic rocks and the Neouvielle pluton were emplaced respectively in Cambrian to Devonian series and in Devonian to Carboniferous metasediments (figure 2). The Neouvielle massif is a late-Carboniferous granodioritic pluton with a high-K calc-alkaline signature characteristic of all the main plutons emplaced in the upper crust during the late Variscan HT-LP event (Debon et al., 1996; Roberts et al., 2000). The pluton is composed of two petrographic facies (Ternet et al., 1995): a light granodiorite in the center of the pluton and a dark granodiorite in its external part. The Chiroulet and Lesponne domes are both made of a metasedimentary series. In the core of the domes, partial melting of the metasediments is recorded by the occurrence of migmatites. Dioritic and granitic bodies appear as intrusions in those migmatites (Pouget, 1984, 1987; Soula et al., 1986; Ternet et al., 1995, 1996). On one hand, the Lesponne dome is divided into two magmatic massifs: the Lesponne *sensu strico* in the west and the Aygue-Rouye massif in the east. However, the continuity of the structures and the petrography shows that they represent the same dome. François (1983) and Pouget (1984) distinguished two different magmatic units. The first magmatic unit is composed of dark granitoids varying in composition from gabbro to granodiorite but mainly consisting of diorite. The second magmatic unit corresponds to light granitoids with a porphyritic granite as the main constituent. While François (1983) proposed that the dark unit is intruded by the light one, Pouget (1984) argued for the opposite. The latter described also an “intermediate facies” between the two units that he interpreted as the result of a mixing between the two magmas. The two units are surrounded by migmatites and by sillimanite bearing schists. On the other hand, the Chiroulet dome is mainly composed of a migmatitic core showing progressive evolution from metatexite to diatexite and anatectic granites from the limbs to the core (Ternet et al., 1996).

3. Methods

3.1. Geochemistry

Bulk-rock composition has been determined by X-ray fluorescence in the Center for Analytical Facility (CAF), Stellenbosch University (South Africa). Analytical method is described in supplementary material appendix A. Major and trace elements and isotopic analyses were obtained in the Service d'Analyse des Roches et des Minéraux (SARM), Nancy (France). Major elements and trace elements were analyzed by ICP-OES and ICP-MS respectively following the analytical procedures described by Carignan et al. (2001). For Sr and Nd isotopic analysis, samples were finely powdered (<50 µm) and digested in a 4:1 HNO_3-HF mixture on a hot plate at 115°C for 48 hours. Following evaporation, samples were rinsed in concentrated HCl and dried. After complete digestion, samples were dissolved in 2 ml 2N HNO_3 then loaded onto Sr Spec and Tru Spec resins for chromatographic separation, following the procedure described in Pin et al. (1994). Sm and Nd fractions were further separated using Ln Spec resin following the procedure described in Pin and Zalduegui (1997). Sr isotopic analysis was performed by thermal ionisation mass spectrometry on a Triton Plus (Thermo electron) apparatus in multicollection static mode. Mass bias was corrected using an exponential law and a $^{86}Sr/^{88}Sr$ reference value of 0.1194. Nd isotopic analysis was performed by MC-ICP-MS on a Neptune Plus (Thermo electron) apparatus. Mass bias was corrected using an exponential law and a $^{146}Nd/^{144}Nd$ reference value of 0.7219.

3.2. Geochronology

A standard mineral separation procedure was applied to concentrate zircon grains using the facilities available at the Géosciences Environnement Toulouse laboratory. Samples were crushed using jaw crusher and disc mill. The powder fraction <400 µm was selected for mineral separation. Zircon grains were concentrated using Wifley table, heavy liquids (tetrabromoethane and diiodomethane) and an isodynamic Frantz separator successively. They were then handpicked under a binocular microscope, embedded in epoxy mount and polished to an equatorial grain section. About 100 to 150 zircon crystals were imaged by cathodoluminescence (CL) using a CAMECA SX-Five at the Centre de Microcaractérisation Raimond Castaing, Toulouse. In order to date partial melting, zircon grains from the migmatites presenting overgrowths were selected. U-Pb analyses were conducted by LA-ICP-MS at Géosciences Rennes using an ESI NWR193UC Excimer laser coupled to a quadripole Agilent 7700x ICP-MS. The instrumental conditions and data processing are reported in appendix B and the procedure follows Ballouard et al. (2015).

3.3. Mineral composition

Biotite composition was measured at the Raimond Castaing Center of the University Paul Sabatier (Toulouse, France), using a CAMECA SX-Five electron microprobe. The operating conditions were as follows: accelerating voltage 15 kV, beam current 20 nA, analysed surface 2x2 µm. The following standards were used: periclase (Mg), corundum (Al), sanidine (K), wollastonite (Si, Ca), pyrophanite (Ti, Mn), hematite (Fe), albite (Na), topaze (F), tugtupite (Cl), $BaSO_4$ (Ba) and Cr_2O_3 (Cr).

4. Field relationships and petrography

4.1. Intrusive magmatic rocks

A light-type (15MSB20) and a dark-type granodiorite (15MSB22) have been sampled in the center and at the margin of the Neouvielle pluton respectively. The light-type granodiorite contains quartz, plagioclase, K-feldspar, rare biotite and rare amphibole and shows HT solid-state deformation (Gleizes et al., 1999). The dark-type granodiorite is composed of quartz, plagioclase, K-feldspar, biotite, hornblende, rare pyroxene and accessory minerals such as zircon and present a poorly defined magmatic fabric.

In the Lesponne dome, one sample (15BL179) has been collected in the dark dioritic unit of the Lesponne sub-dome and one sample (15BL177) has been collected in the light granitic unit of the Aygue Rouye sub-dome. Sample 15BL179 is composed of plagioclase, K-feldspar, biotite, amphibole and rare quartz. It is affected by a foliation (figure 3a) parallel to the regional NW-SE foliation measured in the host micaschists and paragneisses (figure 2c). The mineralogy of sample 15BL177 is quartz, plagioclase, K-feldspar and biotite. The K-feldspar phenocrysts show a shape-preferred orientation (figure 3a-b) which underlines a magmatic foliation related to the emplacement of the granitic body. This magmatic foliation is parallel to the regional foliation recorded in the country rocks. The granitic unit is structurally located above the dioritic unit at the scale of the dome (figure 2c). Foliation planes observed in both units are colinear and parallel to the magmatic contact (figure 3a). The leucogranite and diorite bodies show a similar N130°E magmatic mineral lineation underlined by oriented amphiboles, feldspaths and biotite or muscovite aggregates. Moreover, we locally notice the presence of porphyritic feldspar xenocrysts from the granite inside the dioritic body (figure 3a) at its margin. These observations suggest coeval crystallization for the dioritic and granitic magmas.

In the Chiroulet dome, a granite sample was collected (15BL168) in the core of the structure. It is composed of quartz, plagioclase, K-feldspar, muscovite. We also notice the presence of small amphibolitic enclaves (figure 3c) in the diatexite. One of these enclaves corresponds to sample 15BL166. While some granitic bodies are underformed, others display C/S fabrics (figure 3d) which suggest sub-solidus deformation during or after their emplacement (Gapais, 1989). When observed, the foliation affecting the granitic bodies is parallel to the regional foliation recorded in the migmatites.

4.2. *Migmatites*

The sedimentary rocks of the Lesponne and the Chiroulet domes are both affected by partial melting in the core of the dome. In the Lesponne dome, the migmatites, corresponding to sample 15BL176, are metatexites localized around the magmatic bodies of the Aygue-Rouye dome (figures 2 & 3b). The mineralogy comprises K-feldspar, plagioclase, biotite, sillimanite and biotite. The foliation in the migmatite, underlined by the melanosome-leucosome alternance as well as by the biotite-sillimanite alignment is parallel to the regional foliation. The protolith of these metatexites is supposed to be the

Cambrian metasedimentary unit (Pouget, 1984; Ternet et al., 1995, 1996). Field observations show interconnexion features between migmatite leucosomes and the porphyritic granite (figure 3b). Thus, the porphyritic granite is interpreted as a product of the partial melting of the sediments. In the Chiroulet dome, we sampled the main facies, i.e. migmatitic paragneiss (15BL169) and diatexite (15BL164) close to the anatectic granite (figure 3c-d). The mineralogy of the migmatites is similar to that of the Lesponne migmatites. Similarly to the Lesponne massif, migmatites from the Chiroulet show a well-defined shallowly dipping foliation (figure 3b).

4.3. Metasedimentary sequence

The Lesponne and Chiroulet domes are mantled by Cambrian to Carboniferous metasedimentary rocks. The Cambrian to Ordovician sequence, outcropping in the Lesponne dome, corresponds to andalusite to sillimanite-bearing micaschists (sample 15BL180) and reached partial melting near the Aygue-Rouye granite. The isogrades (figure 2) underline the dome shape and crosscut both the lithologic and the main structural contacts. Dark Silurian schists contain abundant quartz veins in the Lesponne dome. In the northern flank of the Chiroulet dome, the Silurian series is reduced along a detachment level marked by a temperature step from the andalusite bearing Devonian schist to the migmatite (figures 2 and 3; Cochelin, 2016). Devonian rocks are well represented in the studied area and are mainly composed of schists with intercalations of marble. In the Devonian schists from the Lac Bleu area, we noticed the abundance of tourmaline that crystallized within the foliation underlined by quartz ribbons and biotites (figure 3e). The southern flank of the Chiroulet dome is characterized by a northward progressive temperature increase from the biotite to the sillimanite zone. The Carboniferous sediments outcropping in the north of the Neouvielle pluton are limestones and schists. At the contact of the pluton, a metamorphic aureole is superimposed to the epizonal regional metamorphism.

5. Geochemistry

5.1. Major and trace elements chemistry

Results are presented in table 1 and figure 4. In the K_2O vs. SiO_2 diagram (figure 4a), the samples plot in the gabbro-dioritic to granitic fields and all the magmatic rocks from the metamorphic domes and the Neouvielle pluton present the high-K calc-alkaline signature that characterize all the late Variscan plutons in the Pyrenees. Based on the Shand diagram (figure 4b), two rock types are distinguished. The light magmatic rocks, corresponding to the Chiroulet and Lesponne granites and the light granodiorite of the Neouvielle pluton, have a peraluminous signature with A/CNK ratios higher than 1. The Lesponne gabbroic-diorite and the Neouvielle dark granodiorite have a metaluminous signature with A/CNK ratios lower than 1 and higher A/NK ratios than the previous rock type. We note the peculiar position of the Chiroulet amphibolite (15BL166) which has an A/CNK ratio higher than 1 but also a A/NK ratio higher than the light magmatic rocks.

The REE patterns normalized to chondrites (Boynton, 1984) are similar to those measured for other Variscan magmatic rocks in the pyrenean segment with an enrichment in LREE, a slight negative Eu anomaly and a La/Yb ratio in the range of 32 to 7 (figure 4c). The leucogranite and the leucosome of the diatexite of the Chiroulet show distinct patterns characterized by a more depleted spectra when compared to the other samples and La/Yb ratio of 10 and 2 respectively. Extended trace element patterns (figure 4d) normalized to Primitive Mantle (McDonough and Sun, 1995) are characterized by negative anomalies in HFSE (Nb, Ta, Ti) and positive anomalies in LILE (e.g. U, Pb).

5.2. Isotope chemistry

Nd and Sr isotopes analyses have been performed on both magmatic and metasedimentary rocks in order to compare the magmatic signatures with the host rocks and the protoliths of the anatectic granites. The $\varepsilon Nd_{(t)}$ and $^{87}Sr/^{86}Sr_{(t)}$ ratios are recalculated at 300 Ma (mean age obtained by U-Pb dating on zircon - this study) with decay constants from Böhlke et al. (2005) and Steiger and Jäger (1977) respectively and with the chondritic reference value of Bouvier et al. (2008). Results are presented in figure 5. $\varepsilon Nd_{(t)}$ are negative, varying from -2 to -13 and $^{87}Sr/^{86}Sr_{(t)}$ ratios range between 0.702 and 0.720. An evolution from lower $\varepsilon Nd_{(t)}$—higher $^{87}Sr/^{86}Sr_{(t)}$ to higher $\varepsilon Nd_{(t)}$ —lower $^{87}Sr/^{86}Sr_{(t)}$ is observed. While metasedimentary rocks present the most crustal signature (low $\varepsilon Nd_{(t)}$ and high $^{87}Sr/^{86}Sr_{(t)}$), mafic rocks show a signature close to the mantle domain (high $\varepsilon Nd_{(t)}$ and low $^{87}Sr/^{86}Sr_{(t)}$). The granitic rocks of the Lesponne-Chiroulet domes and the Neouvielle granodiorite yield intermediate values between those found for the mafic and metasedimentary rocks.

6. Geochronology

Results and CL images are presented in table 2 and figure 6 respectively. Data have been plotted in Tera Wasserburg Concordia diagrams (figure 7). Concordia ages have been calculated using Isoplot 3.75 (Ludwig, 2012). Uncertainties were propagated following the recommendation from Horstwood et al. (2016) (appendix B).

Zircon grains from the two facies of the Neouvielle granodiorite are colorless and euhedral with sharp concentric zoning (figure 6a and 6b). The analyses of sixteen crystals from the dark facies yield a Concordia age (as of Ludwig, 1998) of 302 ± 2 Ma (MSWD = 0.32; black ellipses in figure 7a) while the Concordia age for the light granodiorite obtained on 17 zircon grains is 305 ± 2 Ma (MSWD = 0.18; grey ellipses in figure 7a).

The zircon crystals from the Lesponne dioritic series are pinkish and elongated. They often present two oscillatory zoned domains separated by a resorption horizon (figure 6c, d, e and f). Two groups of concordant ages are obtained (figure 7b) at 303 ± 3 Ma (MSWD = 0.27; blue ellipses) and 292 ± 2 Ma (MSWD = 0.37; orange ellipses), corresponding to data obtained on internal and external domains respectively in the crystals that present a dissolution horizon. Homogeneous crystals yield either of the two dates. A few analyses (grey ellipses in figure 7b) plot along a horizontal line in the Tera-Wasserburg diagram and return younger $^{206}Pb/^{238}U$ apparent ages. There is no correlation between these younger dates and the position of the laser spot in the corresponding grains. Furthermore, there is no evidence for the presence of outer-rim or overgrowth apart for the ca. 290 Ma ones. Therefore, we interpret these younger dates as meaningless and could be linked to a very slight Pb-loss caused by post-variscan event(s). It is interesting to note that no pre-variscan (i.e. older than 300 Ma) inherited core has been found among the 102 zircon grains imaged by CL for the Lesponne diorite.

In the Lesponne porphyritic granite, two types of zircon grains were found. Type 1 (figure 6g), which is the most abundant, is colorless and elongated with oscillatory zoning in CL images. Type 2 (figure 6h) is brownish and rounded. Type 2 grains present a distinct core surrounded by a narrow rim that could not be analyzed given its small size. The $^{206}Pb/^{238}U$ apparent ages for type 2 zircon cores vary from 650 to 420 Ma (black ellipses in figure 7c). Type 1 zircon analyses plot in a concordant to discordant position (orange and grey ellipses on figure 7c). The oldest group of 15 concordant analyses (orange ellipses) yields a Concordia age of 290 ± 1 Ma (MSWD=0.64; figure 7c). The remaining data (grey ellipses) are sub-concordant to discordant (figure 7c). There is no evidence for recrystallization or overgrowth on the rims of type 1 zircon (figure 6d). Furthermore, there is no specific relationship between the $^{206}Pb/^{238}U$ dates and the position of the analytical laser spot in the grains for the discordant analyses. It is interesting to note that all the analyses younger than 290 Ma plot along a horizontal line in the Tera-Wasserburg diagram. It seems therefore difficult to interpret these younger (i.e < 290 Ma) apparent ages as meaningful, and we rather suggest that they are the consequence of Pb loss. We interpret the data that plot above the Concordia as the consequence of a slight amount of common lead in the crystal lattices. Thus, the scattering of data points might be explained by a combination of common Pb incorporation and slight Pb loss in the 290 Ma old zircon grains that crystallized in the granitic magma.

Zircon crystals in the Lesponne migmatite are euhedral and present distinct cores (figure 6i) yielding apparent $^{206}Pb/^{238}$ ages ranging from 689 to 550 Ma (figure 7d). The cores are resorbed and surrounded by an overgrowth with oscillatory zoning. The concordant analyses from the oldest 11 overgrowths yield a Concordia age of 302 ± 3 Ma (MSWD = 0.72; figure 7d). The analyses obtained on other zircon overgrowths plot in a sub-concordant to discordant position (grey ellipses, figure 7d). Here again, the least discordant analyses present a wide range of apparent $^{206}Pb/^{238}U$ ages as young as 263 Ma (Table 2) and plot along a horizontal line in the Tera-Wasserburg diagram. No evidence for outer rim or overgrowth can be observed on the grains presenting these young $^{206}Pb/^{238}U$ dates. We therefore interpret them as linked to (post carboniferous) Pb loss. The remaining data can be explained by a combination of Pb loss and the presence of variable amount of common Pb in the zircon (Figure 7d).

In the Chiroulet leucogranite, zircon grains are elongated and euhedral, colorless to pinkish, with distinct cores and overgrowth (figure 6j). Cores yield apparent ages ranging from 958 to 470 Ma (Table 2). Analyses performed on the overgrowths plot in concordant to discordant positions (Figure 7e, orange and grey ellipses). The oldest concordant analyses (N=11) yield a Concordia age of 290 ± 3 Ma (MSWD = 1.6; figure 7e, orange ellipses). The remaining data plot either to the right of or above the group of the concordant data. Again, there is no textural evidence to explain the youngest $^{206}Pb/^{238}U$ apparent ages (<290 Ma). We therefore explain the position of those analyses by a combination of Pb loss and the presence of variable amount of common Pb in the zircon (Figure 7e).

Zircon grains of the Chiroulet diatexite are brownish and euhedral. On the CL images, they appear as dark and heterogeneous with the presence of oscillatory zoning at the rim (figure 6k). Uranium content is extremely high (2000 < U(ppm) < 17000). In a Tera Wasserburg diagram (figure 7f), the data plot in a concordant to slightly discordant position with apparent $^{206}Pb/^{238}U$ ages ranging from 297 to 256 Ma. This spread of apparent ages can be best explained by heterogeneous lead loss probably linked to the high uranium contents in the grains (Geisler et al., 2001). The two oldest concordant analyses

(32180117a and 6180117d, table 2) return a Concordia age of 297 ± 6 Ma (MSWD = 0.31) interpreted as the minimum age for the crystallization of these zircon crystals. In that scenario, all the analyses that return younger apparent ages are interpreted as the result of Pb loss. If all the data are taken into account, they yield a poorly defined upper intercept date of 319 +84/- 22 Ma (MSWD = 0.27), which is comparable within error with the date of 297 ± 6 Ma calculated with the two oldest concordant grains. It is interesting to note that none of the imaged grains from this sample presents inherited core.

7. Pressure-temperature estimates

The metamorphic conditions of the host-rock during emplacement of magmatic bodies have been estimated from a sillimanite bearing migmatitic micaschist of the Lesponne dome (sample 15BL176, figure 2). The stable assemblage is Bt-melt-Pl-Sil-Kfs-Qtz (abbreviations from (Kretz, 1983), figure 3f). The Fe/Fe+Mg ratio of biotite is about 0.74. The H_20 content used for phase petrology modelling has been estimated from the loss of ignition. Pseudosections have been drawn in the NCKFMASH system using Perple_X software (Connolly, 2009) with the thermodynamic dataset of Holland and Powell (2004) and solid solution models as detailed in appendix C. Results are presented in figure 8a. The metamorphic assemblage of sample 15BL176 is stable in the range 3.5-6 kbar for a temperature of 650-725 °C, which corresponds to muscovite dehydration melting (figure 8a). The pressure-temperature conditions estimated from the biotite composition are 700 ± 25 °C and 4.2 ± 0.5 kbar.

Chiroulet and Lesponne domes show similarities as they both present a migmatitic core attributed to the late-variscan *HT-LP* metamorphism, synchronous with magmatism and deformation. It is difficult to estimate pressure and temperature for the Chiroulet dome due to i) late pervasive fluid circulation and ii) inappropriate mineralogy (limited to K-feldspar – biotite - quartz) of the metamorphic rocks which hampers the use of geothermetry. However, the greater abundance of diatexite in the Chiroulet dome suggests that melt fraction was higher than in the Lesponne dome. Thus, the maximal temperature reached in the Chiroulet dome may have been higher than in the Lesponne dome. The core of the Chiroulet dome is interpreted as a relic of the middle crust.

The crystallization temperature of a dioritic magma from the Lesponne dome (15BL179) has been estimated using p-Melts software (Ghiorso et al., 2002). As the emplacement depth of the Lesponne diorite and the H_2O content are not well constrained, models have been performed at variable pressure (in the range 3 to 6 kbar corresponding to pressure estimates on the host metamorphic rocks) and variable H_2O content (4 to 8 wt%; Hamilton et al., 1964; Wallace and Anderson, 1999). The aim of these models is to estimate the temperature of crystallization of the last melt and compare it with the temperature of the host-rock. The evolution of the melt fraction as a function of the temperature is represented in figure 8b. The solidus temperature varies from 575 °C (6 kbar, 4 wt% H_2O) to 725 °C (3 kbar, 4 wt% H_2O). The metamorphic temperature recorded in the host-rock (700°C, 4.2 kbar) therefore broadly corresponds to the solidus of the dioritic intrusion. It is thus suggested that the dioritic magmas crystallized in equilibrium with the surrounding metamorphic dome at low depth.

The Neouvielle pluton intruded the low-grade Carboniferous to Devonian metasedimentary series, i.e. within the chlorite zone. Thus, it is advocated that it was emplaced in the upper part of the crust.

8. Discussion

8.1. Petrogenesis of the magmatic rocks

The diversity of the chemical (*e.g.* metaluminous versus peraluminous) and the isotopic characteristics of the magmas ($0.702 < {}^{87}Sr/{}^{86}Sr_{(t)} < 0.716$ and $-13 < \varepsilon Nd_{(t)} < -2$) advocate for the existence of several sources, which could be either (i) mantle peridotites, (ii) magmatic crustal rocks and (iii) metasediments.

(i) Previous studies have suggested that the mantle beneath the Pyrenees was heterogeneous (Fabriès et al., 1998 and references therein). The occurrence of both depleted and enriched mantle is evidenced by the high variability of the εNd for the ultramafic to mafic rocks from different locations in the Pyrenees (Pin, 1989; Roberts et al., 2000).

(ii) The pre-Variscan magmatic rocks outcropping in the Axial Zone are abundant Cambro-Ordovician granites intruding the lower Paleozoic metasediments (Debon et al., 1996). The nature of the underlying lower crust is unknown and some authors infer the presence of basaltic to andesitic lithologies on the basis of petro-geochemical studies of magmatic rocks (Roberts et al., 2000; Kilzi, 2014; Kilzi et al., 2016).

(iii) The Precambrian to Cambro-Ordovician metapelites that constitute the surrounding of the Lesponne dome are characterized by a $^{87}Sr/^{86}Sr$ ratio of 0.718 and a εNd of -10 and are partially molten. Thus, they are considered as a possible source for the magmas. By contrast, the Silurian to carboniferous series in the Pyrenees were never affected by partial melting.

The diorite of the Lesponne dome has the most mafic and the least radiogenic signature of all the analyzed samples, and can be interpreted either as a primary magma issued from the partial melting of a mafic crust or as a mantle derived magma affected by fractional crystallization and crustal contamination. The isotopic signature of the dioritic sample from the Lesponne dome is similar to that of the gabbroic and dioritic rocks analyzed in the Querigut complex by Roberts et al. (2000; figure 5) and interpreted as mantle derived rocks. This signature requires either an enriched mantle source or that the primary magmas have been contaminated by a crustal component. These hypotheses are not mutually exclusive, and both have already been suggested for late-variscan high-K calc-alkaline magmatism in the Pyrenees (Ben Othman et al., 1984; Roberts et al., 2000),in the French Massif Central (Couzinié et al., 2016) or in Sardinia (e.g. Gaggero et al., 2007; Buzzi and Gaggero, 2008; Franciosi et al., 2019). It has been demonstrated elsewhere that the partial melting of a lower crust is responsible for the presence of inherited core in zircon grains found in the melt products (*e.g.* Hansmann and Oberli, 1991; Smyth et al., 2007; Paquette et al., 2010). By contrast, the lack of inherited cores in the zircon grains of the Lesponne diorite indicates that the source of the diorite was zircon-free and supports the hypothesis of a mantle origin. Thus, we propose that the Lesponne diorite results from the emplacement in the metasedimentary crust of a mantle derived magma that experienced crustal contamination. In the Chiroulet dome, fluid circulation is attested by i) peraluminous granite 15BL168 and diatexite leucosome 15BL164 having a Nb/Ta ration lower than 5 (table 1), which is distinctive of peraluminous granites that underwent sub-solidus hydrothermal alteration (Ballouard et al., 2016) and ii) abundance of tourmaline in the Devonian metasediments of the southern flank which highlight the occurrence of metasomatism (Deer et al., 2013). It is well known that fluid circulation combined with metamorphism may induce a change in the A/CNK ratio (*e.g.* Putnis and Austrheim, 2010) and $^{87}Sr/^{86}Sr$ (*e.g.* Dash et al., 1973). Consequently, amphibolite sample 15BL166 of the Chiroulet dome is interpreted as an equivalent of the Lesponne diorite despite its higher A/CNK ratio and lower $^{87}Sr/^{86}Sr$ values (Figure 5).

The peraluminous rocks from the Lesponne and Chiroulet dome are interpreted as the melting product of the Precambrian to Ordovician metasediments as evidenced by their relationships with the migmatites (figure 3f). This hypothesis is further supported by the presence of inherited cores in some of the zircon crystals yielding apparent ages between 960 and 470 Ma. Nevertheless, the isotopic signatures ($0.711 < {}^{87}Sr/{}^{86}Sr_{(t)} < 0.714$ and $-12 < \varepsilon Nd_{(t)} < -6$) lay between the signature of the Precambrian to Ordovician metasediments ($^{87}Sr/^{86}Sr \approx 0.718$, $\varepsilon Nd \approx -10$) and that of the Lesponne diorite. This requires either a mixture of sources or a contamination of the mafic magmas by felsic melts, as evidenced by the contact between the two types of magma in the Lesponne area (figure 3a).

The Neouvielle pluton, emplaced in the Devonian to Carboniferous upper crust, has an isotopic signature intermediate between the Lesponne diorite and the Lesponne metasediments, which suggests a mixed mantle-metasedimentary source. The granodioritic composition, the metaluminous signature of the dark facies and the absence of inherited cores in zircon underlines the mantle contribution. The peraluminous signature of the light facies and its enriched isotopic signatures evidence the sediment contribution, but it remains unclear if these represent sediment assimilation or magma mixing with the products of partial melting in the deep crust.

8.2. *Chronology of the HT-LP event*

U-Pb dating reveal two distinct groups of Concordia ages with weighted averages of 303 ± 1 Ma and 290 ± 3 Ma respectively. The ca. 303 event is recorded in the Neouvielle granodiorite, the Lesponne diorite and the Lesponne—Chiroulet migmatites while the ca. 290 Ma event is recorded in the Lesponne—Chiroulet granites as well as in the Lesponne diorite. The geochronological results show that metamorphic and magmatic activity cover a period of at least 10 My from ca. 303 to 290 Ma. One could interpret these two sets of ages as the result of two magmatic events, with first a crystallization phase of migmatites, granodiorites and diorites at 303 Ma and a minor event at 290 Ma corresponding to the emplacement of leucogranites. However, such an interpretation is in contradiction with some field observations such as i) leucosomes of migmatites and leucogranitic sills in the Lesponne dome share the same petrographic characteristics (figure 3b), ii) the observed progressive transition from migmatites to leucogranites is a feeding contact rather than an intrusive contact, suggesting genetic relationship and synchronous emplacement during deformation and iii) the presence of zircon overgrowths at 290 Ma and a diffuse contact between the Lesponne diorite and granite suggests the coexistence of these two types of magmas (figure 3a). We thus rather suggest a continuous long-lasting magmatic event, extending at least from 303 Ma to 290 Ma. In this scenario, the 303 ± 3 Ma concordant age for diorites is interpreted as its emplacement age within the partially molten middle part of the crust (figure 9a). Indeed, zircon in the migmatites from both the Chiroulet and the Lesponne domes started to crystallize at that time. In detail, in the Lesponne, 11 overgrowths of zircon grains yield a concordant age at 302 ± 3 Ma. In the Chiroulet diatexite, zircon analyses yield a minimum age of 297 ± 6 Ma. Within uncertainty, this minimum age matches the ca. 303 Ma age of the Neouvielle granodiorite and the Lesponne migmatite. It is therefore suggested that the anataxis was initiated at ca. 303 Ma in the middle part of the crust (figure 9a) for both the Lesponne and the Chiroulet domes. At the same time, the Neouvielle granodioritic pluton crystallized in the upper crust at ca. 303 Ma (figure 9a; 305 ± 2 Ma and 302 ± 2 Ma for the light and dark facies respectively). In agreement with structural and petrographic observations, we propose that the deep and middle parts of the crust remained hot and partially molten within the gneiss domes for about at least 10 My from ca. 303 Ma to 290 Ma (figure 9b). Crustal anatexis at 290 Ma is attested by the two well defined groups of concordant ages in the Lesponne porphyritic granite (290 ± 1 Ma) and in the Chiroulet leucogranite (290 ± 3 Ma) that are interpreted as products of the partial melting of the host metasediments. The depleted REE pattern of the Chiroulet leucogranite suggests that it results from multi-stage melt extraction between the onset of the partial melting at ca. 303 Ma and its emplacement at ca. 290 Ma (figure 9b). Dioritic magmatism ended at the same time, as recorded by the youngest concordant age of the Lesponne diorite (292 ± 2 Ma). Phase equilibria modelling (figure 8a) shows that the temperature peak during the late Variscan HT–LP metamorphic event is about 700 °C in the Lesponne—Chiroulet domes, which matches the solidus temperature of the dioritic magmas (figure 8b). It is thus suggested that the Lesponne diorite, emplaced at depth, had remained at a temperature close to its solidus temperature from 303 to 290 Ma. New zircon growth in the partially crystallized magma may have been triggered at 290 Ma by either slight reheating followed by cooling due to a thermal pulse or by a change in magma chemistry, possibly due to magma mixing with the granitic melts. We thus interpret the ca. 290 Ma date recorded in the Lesponne diorite as the crystallization age of the last liquids in the dioritic magma emplaced in the middle part of the crust at ca. 303 Ma (figure 9a and b). By contrast, the Neouvielle granodiorite emplaced at a shallower depth, in a surrounding characterized by a temperature below the solidus and remained fully crystallized since ca. 303 Ma.

8.3. Duration and origin of the late Variscan HT-LP event

The at least 10 My-long HT metamorphic and magmatic activity highlighted by our study in the Chiroulet and Lesponne massifs has been widely documented in the rest of the Axial Zone of the Pyrenees (e.g.

Denèle et al 2014 and references therein). Similar metamorphic-magmatic event, characterized by partially molten metasediments, tonalite and gabbro-diorite intrusions taking place over a timespan of about 10 My was proposed in the Roc de Frausa massif (Aguilar et al., 2014). In the Lys-Caillaouas massif and Bossost dome, the emplacement of plutons occurred around 300-297 Ma, following earlier crystallization of few zircon grains between 320 and 307 Ma possibly due to the initiation of HT-LP metamorphism (Esteban et al., 2015, Lopez-Sanchez et al., 2018). Several studies have evidenced the presence of partially molten crust during periods longer than 10 My in other high temperature terranes (Ashwal et al., 1999; Vanderhaeghe, 2009; Laurent et al., 2018) with multiple stages of zircon crystallization (Harley et al., 2007). Such widespread thermal event at the Carboniferous-Permian transition is consequently not restricted to the Pyrenean crust of the axial zone. High temperature – low pressure metamorphism and associated plutonism also affected the entire southern realm of the Variscan belt (Pin and Vielzeuf, 1983), in the North Pyrenean Massifs (Delaperriere et al., 1994; Olivier et al., 2008; Guille et al., 2018), the Montagne Noire (Poujol et al., 2017), the French Massif Central (e.g. Moyen et al., 2016), the Iberian Massif (Martínez-Catalán et al., 2014), the Alps (e.g. Schuster & Stüwe, 2008; Klötzli et al., 2014; Petri et al., 2017), Sardinia-Corsica-Maures block (e.g. Corsini & Rolland, 2009; Casini et al., 2015; Cocherie et al., 2015; Gaggero et al., 2017), and Calabria (e.g. Graessner et al., 2000; Fornelli et al., 2011). In the Ivrea zone (Kötzli et al., 2017) as well as in the Pyrenees (Pereira et al, 2014), it is recognized that significant mantle derived magmatism takes place at the end of the high temperature metamorphic episode. Because this thermal event affected the foreland of the belt where no major thickening of the crust is recognized (Cochelin et al., 2017), the thermal maturation of a thickened crust cannot be advocated to explain this late metamorphism and an alternative heat source in needed (St Blanquat et al., 1990). Heat advection by intrusion of mafic magma can locally induce thermal anomalies (e.g. De Yoreo et al., 1991), but is unlikely to induce a global scale heating of the crust leading to anatexis. Moreover, in the absence of recognized water influx that would lower mantle solidus, the initiation of partial melting in the mantle itself requires either mantle upwelling or heating, which would correspond in any case to an increase of the thermal mantle flux at the base of the crust. Geodynamic processes such as thermal erosion or delamination of lithospheric mantle can be advocated here (Denèle et al., 2014, Cochelin et al., 2017). The latter is supposed to have taken place within the hinterland of the belt after 340-330 Ma (Armorican Massif, see Gapais et al. 2015, Ballouard et al., 2017; Iberian Massif, see Martínez-Catalán et al 2014; French Massif Central, see Laurent et al., 2017). Southward propagation of magmatism and metamorphism from the hinterland to the foreland of the belt in the French Massif Central until ca. 300 Ma was interpreted as the response to slab rollback leading to the delamination of the lithospheric mantle by Laurent et al. (2017). This interpretation is challenged by our geochronological data, that shows that the magmatic activity in the Pyrenees is coeval with that in the south of the Massif Central, despite its southern foreland position. We thus propose that the initiation of metamorphism and bimodal magmatism at ca. 305 Ma in the Axial Zone is the expression of the delamination of the Gondwanan lithospheric mantle at a global scale in the Variscan belt. This interpretation is supported by recent structural study showing that the Pyrenees was an abnormally hot foreland of the Variscan belt, showing deformation patterns typical of hot orogens in a context of missing lithospheric mantle (Cochelin et al., 2017). The continuation of magmatism (e.g. high-K plutonism and volcanism) in an extensional context during Permian times in the Pyrenees (Lago et al., 2004; Denèle et al., 2012, Pereira et al., 2014), Alps (Köztli et al., 2014; Petri et al., 2017; Manzotti et al., 2018), Corsica-Sardinia (Corsini & Rolland, 2009; Casini et al., 2015; Cocherie et al., 2015; Rossi et al., 2015; Gaggero et al., 2007; 2017) and Iberia (Martínez-Catalán et al., 2014; Casini et al., 2015) illustrates the persistence of i) the thermal anomaly and ii) an attenuated lithosphere, which may have favor the break-up of Pangea at this period.

9. Conclusion

Our results provide new petrological and U-Pb chronological constraints on the late Variscan high-K calc-alkaline magmatism and HT-LP metamorphism in the Chiroulet-Lesponne-Neouvieille zone in the western Axial Zone of the Pyrenees.

Two magma sources have been recognized, a mantle source that produced metaluminous magmas best exemplified by the Lesponne diorite and a metasedimentary source that produced peraluminous magmas like the Chiroulet and Lesponne granite and evidenced by the presence of migmatites.

Magmatism took place over a period of about 10-15 My, with two peaks at 303 Ma and 290 Ma, recorded in both magma types. It is therefore shown that there is no time delay between mantle magmas intrusion and the beginning of partial melting in the crust. The coexistence of the two magma types induced magma mixing attested by field observations and intermediate chemical and isotopic signatures.

While the magmas crystallized at ca. 303 Ma in the upper crust, forming the Neouvielle pluton, the middle crust remained partially molten with occurrences of both mantle and crustal magmas persisting for about 10 My. At ca. 290 Ma, the middle crust cooled down inducing the final crystallization of the magmas emplaced in gneiss domes.

The abundance of high K calc-alkaline magmas associated with crustal partial melting and the presence of HT-LP metamorphism are in favor of a geodynamic context 1) without crustal thickening 2) during a late orogenic phase. Consequently, the late Variscan HT-LP event necessitates a mantle source and cannot be explained by thermal maturation of a thickened crust. This also significates that the late Variscan event lasted at least about 10-15 My until the beginning of the Permian time. We propose that the initiation of metamorphism and bimodal magmatism at ca. 305 Ma in the Pyrenees is the expression of the delamination of the Gondwanan lithospheric mantle at a global scale in the Variscan belt.

Acknowledgments

This work was supported by the BRGM through the Référentiel Géologique de la France (RGF) program. BC acknowledges funding from Labex Voltaire (ANR-10-LABX-100-01), based at Orléans University and BRGM. The authors warmly want to thank Valerie Bosse, Oscar Laurent and Laura Gaggero for their insightful comments on a previous version of this manuscript as well as Xian-Hua Li for his editorial handling.

References

Aguilar, C., Montserrat, L., Castiñeiras, P., Navidad, M., 2014. Late Variscan metamorphic and magmatic evolution in the eastern Pyrenees revealed by U-Pb age zircon dating. J. Geol. Soc. London 171, 181–192.

Ashwal, L.D., Tucker, R.D., Zinner, E.K., 1999. Slow cooling of deep crustal granulites and Pb-loss in zircon. Geochim. Cosmochim. Acta 63, 2839–2851. https://doi.org/10.1016/S0016-7037(99)00166-0

Azambre, B., Guitard, G., 2001. Disthène et staurotide reliques dans les métapelites du Canigou (Pyrénées orientales). Relations avec les épisodes hercyniens de basse et moyenne pressions. Comptes Rendus l'Académie des Sci. - Ser. IIA - Earth Planet. Sci. 333, 601–609. https://doi.org/10.1016/S1251-8050(01)01670-6

Ballouard, C., Boulvais, P., Poujol, M., Gapais, D., Yamato, P., Tartèse, R., Cuney, M., 2015. Tectonic record, magmatic history and hydrothermal alteration in the Hercynian Guérande leucogranite, Armorican Massif, France. Lithos 220–223, 1–22. https://doi.org/10.1016/J.LITHOS.2015.01.027

Ballouard, C., Poujol, M., Boulvais, P., Branquet, Y., Tartèse, R., Vigneresse, J.L., 2016. Nb-Ta fractionation in peraluminous granites: A marker of the magmatic-hydrothermal transition. Geology 44, 231–234.

https://doi.org/10.1130/G37475.1

Ballouard, C., Poujol, M., Boulvais, P., Zeh, A., 2017. Crustal recycling and juvenile addition during lithospheric wrenching: The Pontivy-Rostrenen magmatic complex, Armorican Massif (France), Variscan belt. Gondwana Research 49, 222-247. http://dx.doi.org/10.1016/j.gr.2017.06.002

Ben Othman, D., Fourcade, S., Allègre, C.J., 1984. Recycling processes in granite-granodiorite complex genesis: the Querigut case studied by NdSr isotope systematics. Earth Planet. Sci. Lett. 69, 290–300. https://doi.org/10.1016/0012-821X(84)90188-2

Böhlke, J., De Laeter, J., De Bievre, P., Hidaka, H., Peiser, H., Rosman, K., Taylor, P., 2005. Isotopic compositions of the elements, 2001. J. Phys. Chem. Ref. Data 34, 57–67.

Bonin, B., 2004. Do coeval mafic and felsic magmas in post-collisional to within-plate regimes necessarily imply two contrasting, mantle and crustal, sources? A review. Lithos 78, 1–24. https://doi.org/10.1016/j.lithos.2004.04.042

Bosse, V., Feraud, G., Ruffet, G., Ballèvre, M., Peucat, J.-J., De Jong, K., 2000. Late Devonian subduction and early-orogenic exhumation of eclogite-facies rocks from the Champtoceaux Complex (Variscan belt, France). Geol. J. 35, 297–325.

Bouvier, A., Vervoort, J.D., Patchett, P.J., 2008. The Lu-Hf and Sm-Nd isotopic composition of CHUR: Constraints from unequilibrated chondrites and implications for the bulk composition of terrestrial planets. Earth Planet. Sci. Lett. 273, 48–57. https://doi.org/10.1016/j.epsl.2008.06.010

Boynton, W. V, 1984. Cosmochemistry of the rare earth elements: meteorite studies. Dev. geochemistry 63–114.

Burg, J.-P., Van den Driessche, J., Brun, J.-P., 1994. Syn-to post-thickening extension in the Variscan Beit of Western Europe: Modes and structural consequences. Géologie la Fr.

Burg, J.P., Gerya, T. V., 2005. The role of viscous heating in Barrovian metamorphism of collisional orogens: Thermomechanical models and application to the Lepontine Dome in the Central Alps. J. Metamorph. Geol. 23, 75–95. https://doi.org/10.1111/j.1525-1314.2005.00563.x

Buzzi, L., & Gaggero, L., 2008. Petrogenesis of post – orogenic Lower Permian andesites in southern Europe: insights into the collapse of the Variscan range, Geodinamica Acta, 21, 5-6, 273-290, https://doi.org/10.3166/ga.21.273-290

Carignan, J., Hild, P., Mevelle, G., Morel, J., Yeghicheyan, D., 2001. Routine Analyses of trace Elements in Geological Samples using Flow injection and Low Pressure On-Line liquid Chromatography Coupled to ICP-MS : A study of Geochemical Reference Materials BR, DR-N, UB-N, AN-G and GH. Geostand. Newsl. 25, 187–198. https://doi.org/10.1111/j.1751-908X.2001.tb00595.x

Carreras, J., Debat, P., 1996. Tectonique hercynienne, in: Synthèse Géologique et Géophysique Des Pyrénées. pp. 585–677.

Casini, L., Cuccuru, S., Puccini, A., Oggiano, G., Rossi, Ph., 2015. Evolution of the Corsica-Sardinia Batholith and late-orogenic shearing of the Variscides. Tectonophysics 646, 65-78. http://dx.doi.org/10.1016/j.tecto.2015.01.017

Cochelin, B., 2016. Champ de déformation du socle paléozoïque des Pyrénées. PhD thesis, Toulouse (France), Univ. Paul Sabatier.

Cochelin, B., Chardon, D., Denèle, Y., Gumiaux, C., Le Bayon, B., 2017. Vertical strain partitioning in hot Variscan crust: Syn-convergence escape of the Pyrenees in the Iberian-Armorican syntax. Bull. la Société géologique Fr. 188, 39. https://doi.org/10.1051/bsgf/2017206

Cochelin, B., Lemirre, B., Denèle, Y., De Saint Blanquat, M., Lahfid, A., Duchêne, S., 2018. Structural inheritance in the Central Pyrenees : the Variscan to Alpine tectonometamorphic evolution of the

Axial Zone. J. Geol. Soc. London. 175, 336–351. https://doi.org/10.1144/jgs2017-066

Cocherie, A., Rossi, P., and Fanning, C.M., 2015, Evidence in Variscan Corsica of a brief and voluminous Late Carboniferous to Early Permian volcanic-plutonic event contemporaneous with a high-temperature/low-pressure metamorphic peak in the lower crust: Bulletin de la Société Géologique de France, v. 186, p. 171-192

Connolly, J. a D., 2009. The geodynamic equation of state: What and how. Geochemistry, Geophys. Geosystems 10. https://doi.org/10.1029/2009GC002540

Corsini, M. and Rolland, Y., 2009. Late evolution of the southern European Variscan belt: Exhumation of the lower crust in a context of oblique convergence. Comptes Rendus Geoscience 341, 214-223. https://doi.org/10.1016/j.crte.2008.12.002.

Couzinié, S., Laurent, O., Moyen, J.-F., Zeh, A., Bouilhol, P., Villaros, A., 2016. Post-collisional magmatism: Crustal growth not identified by zircon Hf–O isotopes. Earth Planet. Sci. Lett. 456, 182–195. https://doi.org/10.1016/j.epsl.2016.09.033

Dash, E.J., Hedge, C.E., Dymond, J., 1973. Effect of sea water interaction on strontium isotope composition of deep-sea basalts. Earth Planet. Sci. Lett. 19, 177–183.

De Yoreo, J.J., Lux, D.R., Guidotti, C. V, 1991. Thermal modelling in low-pressure/high-temperature metamorphic belts. Tectonophysics 188, 209–238.

Debon, F., Enrique, P., Autran, A., 1996. Magmatisme hercynien, in: Synthèse Géologique et Géophysique Des Pyrénées. pp. 361–499.

Deer, W.A., Howie, R.A., Zussman, J., 2013. An Introduction to the Rock-Forming Minerals. Third edition.

Delvolvé, J.J., 1996. Carbonifère à faciès Culm, in: Synthèse Géologique et Géophysique Des Pyrénées. pp. 303–338.

Denèle, Y., Laumonier, B., Paquette, J.-L., Olivier, P., Gleizes, G., Barbey, P., 2014. Timing of granite emplacement, crustal flow and gneiss dome formation in the Variscan segment of the Pyrenees. Geol. Soc. London, Spec. Publ. 405, 265–287. https://doi.org/10.1144/SP405.5

Denèle, Y., Paquette, J.-L., Olivier, P., Barbey, P., 2011. Permian granites in the Pyrenees: the Aya pluton (Basque Country). Terra Nov. 24, 105–113. https://doi.org/10.1111/j.1365-3121.2011.01043.x

Depine, G. V, Andronicos, C.L., Phipps-Morgan, J., 2008. Near-isothermal conditions in the middle and lower crust induced by melt migration. Nature 452, 80–83. https://doi.org/10.1038/nature06689

Druguet, E., Castro, A., Chichorro, M., Pereira, M.F., Fernández, C., 2014. Zircon geochronology of intrusive rocks from Cap de Creus, Eastern Pyrenees. Geol. Mag. 151, 1095–1114. https://doi.org/10.1017/S0016756814000041

England, P.C., Thompson, A.B., 1984. Pressure-temperature-time paths of regional metamorphism I. Heat transfer during the evolution of thickened continental crust. J. Petrol. 25, 894–928.

Esteban, J.J., Aranguren, A., Cuevas, J., Hilario, A., Tubía, J.M., Larionov, A., Sergeev, S., 2015. Is there a time lag between the metamorphism and emplacement of plutons in the Axial Zone of the Pyrenees? Geol. Mag. 152, 935–941. https://doi.org/10.1017/S001675681500014X

Fabriès, J., Lorand, J.P., Bodinier, J.L., 1998. Petrogenetic evolution of orogenic lherzolite massifs in the central and western Pyrenees. Tectonophysics 292, 145–167. https://doi.org/10.1016/S0040-1951(98)00055-9

Fornelli, A., Langone, A., Micheletti, A.-M., and Piccarreta, G., 2011, Time and duration of Variscan high-temperature metamorphic processes in the south European Variscides: constraints from U-Pb chronology and trace element chemistry of zircon: Mineralogy and Petrology, v. 103, p. 101–122.

Franciosi, L., D'Antonio, M., Fedele, L., Guarino, V., Tassinari, C. C. G., de Gennaro, R., Cucciniello, C.,

2019. Petrogenesis of the Solanas gabbro-granodiorite intrusion, Sàrrabus (southeastern Sardinia, Italy): implications for Late Variscan magmatism. Int. J. Earth Sci. https://doi.org /10.1007/s00531-019-01689-8

François, J.M., 1983. Etude géologique et métallogénique de la région du Pic du Midi de Bigorre (Hautes-Pyrénées). PhD thesis, Univ. of Nancy (France).

Franke, W., 2014. Topography of the Variscan orogen in Europe: Failed-not collapsed. Int. J. Earth Sci. 103, 1471–1499. https://doi.org/10.1007/s00531-014-1014-9

Franke, W., Doublier, M.P., Klama, K., Potel, S., Wemmer, K., 2011. Hot metamorphic core complex in a cold foreland. Int. J. Earth Sci. 100, 753–785. https://doi.org/10.1007/s00531-010-0512-7

Gaggero, J., Oggiano, G., Buzzi, L., Slejko, F., Cortesogno, L., 2007. Post-Variscan mafic dikes from the late orogenic collapse to the Tethyan rift: evidence from Sardinia. Ofioliti, 32, 15-37.

Gaggero, L., Gretter, N., Langone, A., Ronchi, A., 2017. U-Pb geochronology and geochemistry of late Paleozoic in Sardinia (southern Variscides). Geoscience Frontiers, 8, 1263-1284. http://dx.doi.org/10.1016/j.gsf.2016.11.015

Gapais, D., 1989. Shear structures within deformed granites: mechanical and thermal indicators. Geology 17, 1144–1147. https://doi.org/10.1130/0091-7613(1989)017<1144:SSWDGM>2.3.CO;2

Gapais, D., Brun, J.-P., Gumiaux, C., Cagnard, F., Ruffet, G., Le Carlier De Veslud, C., 2015. Extensional tectonics in the Hercynian Armorican belt (France). An overview. Bull. Soc. Géol. Fr. 186, 117–129. https://doi.org/10.2113/gssgfbull.186.2-3.117

Geisler, T., Ulonska, M., Schleicher, H., Pidgeon, R. T., van Bronswijk, W., 2001. Leaching and differential recrystallization of metamict zircon under experimental hydrothermal conditions. Contrib. to Min. and Pet. 141, 53-65.

Ghiorso, M.S., Hirschmann, M.M., Reiners, P.W., Kress, V.C., 2002. The pMELTS: A revision of MELTS for improved calculation of phase relations and major element partitioning related to partial melting of the mantle to 3 GPa. Geochemistry, Geophys. Geosystems 3, 1–35. https://doi.org/10.1029/2001GC000217

Giacomini, F., Bomparola, R.M., Ghezzo, C., Guldbransen, H., 2006. The geodynamic evolution of the Southern European Variscides: constraints from the U/Pb geochronology and geochemistry of the lower Palaeozoic magmatic-sedimentary sequences of Sardinia (Italy). Contrib. to Mineral. Petrol. 152, 19.

Guille, B. T., Olivier, P., Paquette, J. L., Bosse, V., Guillaume, D., 2018. Evolution of the middle crust of the Pyrenees during the Paleozoic: new data on the plutonic rocks from the North Pyrenean Agly Massif. Int. J. Earth Sci. https://doi.org /10.1007/s00531-018-1652-4

Guitard, G., Vielzeuf, D., Martinez, F., 1996. Métamorphisme hercynien. Synthèse Géologique Géophysique des Pyrénées 501–584.

Gutiérrez-Alonso, G., Fernández-Suárez, J., Jeffries, T.E., Johnston, S.T., Pastor-Galán, D., Murphy, J.B., Franco, M.P., Gonzalo, J.C., 2011. Diachronous post-orogenic magmatism within a developing orocline in Iberia, European Variscides. Tectonics 30, 1–17. https://doi.org/10.1029/2010TC002845

Hamilton, D.L., Burnham, C.W., Osborn, E.F., 1964. The Solubility of Water and Effects of Oxygen Fugacity and Water Content on Crystallization. J. Petrol. 5, 21–39. https://doi.org/10.1093/petrology/5.1.21

Hansmann, W., Oberli, F., 1991. Zircon inheritence in an igneous rock suite of the Soutehrn Adamello batholith (Italien Alps): Implication for petrogenesis. Contr. Mineral. and Petrol. 107, 501–518. https://doi.org /10.1007/BF00310684

Harley, S.L., Kelly, N.M., Möller, A., 2007. Zircon behaviour and the thermal history of mountain belts.

Elements 3, 25–30. https://doi.org/10.2113/gselements.3.1.25

Henk, A., von Blanckenburg, F., Finger, F., Schaltegger, U., Zulauf, G., 2000. Syn-convergent high-temperature metamorphism and magmatism in the Variscides : a discussion of potential heat sources. Geol. Soc. London, Spec. Publ. 179, 387–399.

Holland, T.J.B., Powell, R., 2004. An internally consistent thermodynamic data set for phases of petrological interest. J. Metamorph. Geol. 16, 309–343. https://doi.org/10.1111/j.1525-1314.1998.00140.x

Horstwood, M. S., Kosler, J., Gehrels, G., Jackson, S. E., McLean, N. M., Paton, C., Pearson, N. J., Sircombe, K., Syvester, P., Vermeesch, P., Bowring, J. F., Condon, D. J., Schoene, B., 2016. Community derived standards for LA-ICP-MS U-(Th)-Pb geochronology - Uncertainty propagation, age interpretation and data reporting. Geostandards and Geoanalytical Research 40 (3), 311-332.

Kilzi, M., 2014. Roches ultramafiques de Gavarnie et de Castillon. Phd thesis, Université de Toulouse. https://doi.org/10.1163/187122099X00065

Kilzi, M.A., Grégoire, M., Bosse, V., Benoît, M., Driouch, Y., de Saint Blanquat, M., Debat, P., 2016. Geochemistry and zircon U–Pb geochronology of the ultramafic and mafic rocks emplaced within the anatectic series of the Variscan Pyrenees: The example of the Gavarnie–Heas dome (France). Comptes Rendus Geosci. 348, 107–115. https://doi.org/10.1016/J.CRTE.2015.06.014

Klötzli, U.S., Sinigoi, S., Quick, J.E., Demarchi, G., Tassinari, C.C.G., Sato, K., and Günes, Z., 2014, Duration of igneous activity in the Sesia Magmatic System and implications for high-temperature metamorphism in the Ivrea–Verbano deep crust: Lithos, v. 206-207, p. 19-33.

Kretz, R., 1983. Symbols for rock-forming minerals. Am. Mineral. 68, 277–279. https://doi.org/10.1016/0016-7037(83)90220-X

Lago, M., Arranz, E., Pocoví, A., Galé, C., Gil-Imaz, A., 2004. Permian magmatism and basin dynamics in the southern Pyrenees: A record of the transition from late Variscan transtension to early Alpine extension, in Wilson, M., et al., eds., Permo-Carboniferous magmatism and rifting in Europe. Geol. Soci. Spec. Pub. 223, p. 439–464, https://doi.org/10.1144/GSL.SP.2004.223.01.19

Lardeaux, J.M., 2014. Deciphering orogeny: A metamorphic perspective examples from european alpine and variscan belts Part II: Variscan metamorphism in the french massif central - A review. Bull. Soc. Geol. Fr. 185, 281–310. https://doi.org/10.2113/gssgfbull.185.2.93

Laurent, A.T., Bingen, B., Duchene, S., Whitehouse, M.J., Seydoux-Guillaume, A., Bosse, V., 2018. Decoding a protracted zircon geochronological record in ultrahigh temperature granulite, and persistence of partial melting in the crust, Rogaland, Norway. Contrib. to Mineral. Petrol. 173, 29.

Laurent, O., Couzinié, S., Zeh, A., Vanderhaeghe, O., Moyen, J.-F., Villaros, A., Gardien, V., Chelle-Michou, C., 2017. Protracted, coeval crust and mantle melting during Variscan late‐orogenic evolution: U–Pb dating in the eastern French Massif Central. Int. J. Earth Sci. 106, 421-451. https://doi.org/10.1007/s00531-016-1434-9

Lopez-Sanchez M.A., García-Sansegundo J., Martínez F.J., 2018. The significance of early Permian and early Carboniferous U–Pb zircon ages in the Bossòst and Lys-Caillaouas granitoids (Pyrenean Axial Zone). Geological Journal 1–16. https://doi.org/10.1002/gj.3283

Lotout, C., Pitra, P., Poujol, M., Anczkiewicz, R., Van Den Driessche, J., 2018. Timing and duration of Variscan high-pressure metamorphism in the French Massif Central: A multimethod geochronological study from the Najac Massif. Lithos 308–309, 381–394. https://doi.org/10.1016/j.lithos.2018.03.022

Ludwig, K., 2012. User's manual for Isoplot version 3.75--4.15: a geochronological toolkit for Microsoft.

Excel Berkley Geochronological Cent. Spec. Publ.

Ludwig, K.R., 1998. On the treatment of concordant uranium-lead ages. Geochim. Cosmochim. Acta 62, 665–676. https://doi.org/10.1016/S0016-7037(98)00059-3

Manzotti, P., Rubatto, D., Zucali, M., El Korh, A., Cenki-Tok, B., Ballèvre, M., Engi, M., 2018. Permian magmatism and metamorphism in the Dent Blanche nappe: constraints from field observations and geochronology. Swiss J. Geosci. 11, 79–97. https://doi.org/10.1007/s00015-017-0284-1

Martínez Catalán, J.R., 2011. Are the oroclines of the Variscan belt related to late Variscan strike-slip tectonics? Terra Nov. 23, 241–247. https://doi.org/10.1111/j.1365-3121.2011.01005.x

Martínez-Catalán, J.R., Pascual, F.J.R, Montes, A.D., Fernández, R.D., Barreiro, J.G., Silva, Í.D.D., et al. 2014. The late Variscan HT/LP metamorphic event in NW and Central Iberia: relationships to crustal thickening, extension, orocline development and crustal evolution. Geol. Soc. Spec. Publ. 405, 225–247. http://dx.doi.org/10.1144/SP405.1

Matte, P., 2001. The Variscan collage and orogeny (480 ± 290 Ma) and the tectonic definition of the Armorica microplate : a review. Terra Nov. 13, 122–128.

Matte, P., 1991. Accretionary history and crustal evolution of the Variscan belt in Western Europe. Tectonophysics 196, 309–337. https://doi.org/10.1016/0040-1951(91)90328-P

McDonough, W.F., Sun, S. -s., 1995. The composition of the Earth. Chem. Geol. 120, 223–253. https://doi.org/10.1016/0009-2541(94)00140-4

Mezger, J.E., Passchier, C.W., Régnier, J.-L., 2004. Metastable staurolite–cordierite assemblage of the Bossòst dome: Late Variscan decompression and polyphase metamorphism in the Axial Zone of the central Pyrenees. Comptes Rendus Geosci. 336, 827–837. https://doi.org/10.1016/j.crte.2003.12.024

Mezger, J.E., Wissenschaften, G., 2005. Comparison of the western Aston-Hospitalet and the Bossòst domes : Evidence for polymetamorphism and its implications for the Variscan tectonic evolution of the Axial Zone of the Pyrenees. J. Virtual Explor. 19, 1–19.

Middlemost, E., 1985. Magmas and magmatic rocks: an introduction to igneous petrology. Longman London.

Moyen, J.-F., Laurent, O., Chelle-Michou, C., Couzinié, S., Vanderhaeghe, O., Zeh, A., Villaros, A., Gardien, V., 2017. Collision vs. subduction-related magmatism: Two contrasting ways of granite formation and implications for crustal growth. Lithos 277, 154-177, http://dx.doi.org/10.1016/j.lithos.2016.09.018

O'Brien, P.J., 2000. The fundamental Variscan problem: high-temperature metamorphism at different depths and high-pressure metamorphism at different temperatures. Geol. Soc. London, Spec. Publ. 179, 369–386.

Olivier, P., Gleizes, G., Paquette, J.L., and Munoz-Saez, C., 2008, Structure and U–Pb dating of the Saint-Arnac pluton and the Ansignan charnockite (Agly Massif): a cross-section from the upper to the middle crust of the Variscan Eastern Pyrenees: Journal of the Geological Society of London, v. 165, p. 41–152.

Padel, M., Álvaro, J.J., Casas, J.M., Clausen, S., Poujol, M., Sánchez-García, T., 2018. Cadomian volcanosedimentary complexes across the Ediacaran–Cambrian transition of the Eastern Pyrenees, southwestern Europe. Int. J. Earth Sci. 107, 1579–1601. https://doi.org/10.1007/s00531-017-1559-5

Paquette, J.-L., Ballèvre, M., Peucat, J.-J., Cornen, G., 2017. From opening to subduction of an oceanic domain constrained by LA-ICP-MS U-Pb zircon dating (Variscan belt, Southern Armorican Massif, France). Lithos 294–295, 418–437. https://doi.org/10.1016/J.LITHOS.2017.10.005

Paquette, J., de Saint Blanquat, M., Delpech, G., Horsman, E., Morgan, S., 2010. LA-ICPMS U-Pb zircon dating of Mount Hiller laccolite and satellite intrusions: shortlength emplacement and large Proterozoic inheritance. Laccoliths Sills Int. 4 Conf. Abstr. Henry Mt. Utah.

Peccerillo, A., Taylor, S.R., 1976. Geochemistry of Eocene cale-alkaline volcanic rocksfrom the Kastamonu Area, Northern Turkey. Contrib. to Mineral. Petrol. 58, 63–81.

Pereira, M.F., Castro, a., Chichorro, M., Fernández, C., Díaz-Alvarado, J., Martí, J., Rodríguez, C., 2014. Chronological link between deep-seated processes in magma chambers and eruptions: Permo-Carboniferous magmatism in the core of Pangaea (Southern Pyrenees). Gondwana Res. 25, 290–308. https://doi.org/10.1016/j.gr.2013.03.009

Petri, B., Mohn, G., Skrzypek, E., Mateeva, T., Galster, F., Manatschal, G., 2017. U–Pb geochronology of the Sondalo gabbroic complex (Central Alps) and its position within the Permian post-Variscan extension. Int. J. Earth Sci. 106, 2873-2893. https://doi.org/10.1007/s00531-017-1465-x

Pin, C., 1989. Essai sur la chronologie et l'évolution géodynamique de la chaîne Hercynienne d'Europe. PhD thesis, Clermont-ferrand (France), Univ. Blaise Pascal.

Pin, C., Vielzeuf, D., 1983. Granulites and related rocks in variscan median Europe: a dualistic interpretation. Tectonophysics 93, 47‑74.

Pin, C., Briot, D., Bassin, C., and Poitrasson, F., 1994, Concomitant separation of strontium and samarium-neodymium for isotopic analysis in silicate samples, based on specific extraction chromatography: Analytica Chimica Acta, v. 298, p. 209-217.

Pin, C., and Zalduegui, J.S., 1997, Sequential separation of light rare-earth elements, thorium and uranium by miniaturized extraction chromatography: Application to isotopic analyses of silicate rocks: Analytica Chimica Acta, v. 339, p. 79-89.

Pouget, P., 1987. Le Massif Granatique de Lesponne (High Pyrenees): en exemple de Massif Plutonique Hercynien a mise en place diapirque Syncinematique. Granites - Geol. Runschen. 76, 187–201.

Pouget, P., 1984. Géologie de la région de Lesponne (Hautes-Pyrénées), PhD Thesis, Toulouse (France), Univ. Paul Sabatier.

Poujol, M., Pitra, P., van Den Driessche, J., Tartèse, R., Ruffet, G., Paquette, J.L., Poilvet, J.C., 2017. Two-stage partial melting during the Variscan extensional tectonics (Montagne Noire, France). Int. J. Earth Sci. 106, 477–500. https://doi.org/10.1007/s00531-016-1369-1

Putnis, A., Austrheim, H., 2010. Fluid-Induced Processes: Metasomatism and Metamorphism. Front. Geofluids 10, 254–269. https://doi.org/10.1002/9781444394900.ch18

Riel, N., Mercier, J., Weinberg, R., 2016. Convection in a partially molten metasedimentary crust? Insights from the El Oro complex (Ecuador). Geology 44, 31–34. https://doi.org/10.1130/G37208.1

Roberts, M.P., Pin, C., Clemens, J.D., Paquette, J., 2000. Petrogenesis of Mafic to Felsic Plutonic Rock Associations : the Calc-alkaline Querigut Complex , French Pyrenees. J. Petrol. 41, 809–844.

Roger, F., Matte, P., 2005. Early Variscan HP metamorphism in the western Iberian Allochthon—A 390 Ma U--Pb age for the Bragança eclogite (NW Portugal). Int. J. Earth Sci. 94, 173–179.

Rossi, P., Cocherie, A., Fanning, C.M., 2015. Evidence in Variscan Corsica of a brief and voluminous Late Carboniferous to Early Permian volcanic-plutonic event contemporaneous with a high-temperature/low-pressure metamorphic peak in the lower crust. Bull. Soc. géol. France 186, 171-192.

Saint Blanquat, M., Lardeaux, J.M., Brunel, M., 1990. Petrological arguments for high temperature extensional deformation in the Pyrenean Variscan crust (Saint Barthélémy Massif, Ariège, France). Tectonophysics 177, 245–262.

Schulmann, K., Oliot, E., Košuličová, M., Montigny, R., Štípská, P., 2014. Variscan thermal overprints exemplified by U-Th-Pb monazite and K-Ar muscovite and biotite dating at the eastern margin of the Bohemian Massif (East Sudetes, Czech Republic). J. Geosci. (Czech Republic) 59, 389–413. https://doi.org/10.3190/jgeosci.180

Schuster R. and Stüwe K., 2008. Permian metamorphic event in the Alps. Geology 36, 603-606. doi:10.1130/G24703A.1

Shand, S.J., 1943. Eruptive rocks. Their genesis, composition, classification, and their relations to ore-deposits. Wiley, New York.

Smyth, H.R., Hamilton, P.J., Hall, R., Kinny, P.D., 2007. The deep crust beneath island arcs: Inherited zircons reveal a Gondwana continental fragment beneath East Java, Indonesia. Earth Planet. Sci. Lett. 258, 269–282. https://doi.org/10.1016/j.epsl.2007.03.044

Soula, J.-C., Debat, P., Déramond, J., Guchereau, J.-Y., Lamouroux, C., Pouget, P., Roux, L., 1986. Evolution structurale des ensembles métamorphiques, des gneiss et des granitoïdes dans les Pyrénées centrales. Bull. Soc. Geol. Fr. 8, 79–93.

Steiger, R., Jäger, E., 1977. Subcommission on geochronology: convention on the use of decay constants in geo-and cosmochronology. Earth Planet. Sci. Lett. 36, 359–362.

Ternet, Y., Barrère, P., Dallas, S., Debon, F., Debroas, E.J., François, J.M., Pouget, P., 1996. Carte géologique de France (1/50 000), feuille Campan (1071). BRGM.

Ternet, Y., Barrère, P., Debroas, E.J., 1995. Notice explicative, Carte géologique de France (1/50 000), feuille Campan (1071). BRGM.

Vacherat, A., Mouthereau, F., Pik, R., Huyghe, D., Paquette, J.-L., Christophoul, F., Loget, N., Tibari, B., 2017. Rift-to-collision sediment routing in the Pyrenees: A synthesis from sedimentological, geochronological and kinematic constraints. Earth-Science Rev. 172, 43–74. https://doi.org/10.1016/J.EARSCIREV.2017.07.004

Vanderhaeghe, O., 2012. The thermal-mechanical evolution of crustal orogenic belts at convergent plate boundaries: A reappraisal of the orogenic cycle. J. Geodyn. 56–57, 124–145. https://doi.org/10.1016/j.jog.2011.10.004

Vanderhaeghe, O., 2009. Migmatites, granites and orogeny: Flow modes of partially-molten rocks and magmas associated with melt/solid segregation in orogenic belts. Tectonophysics 477, 119–134. https://doi.org/10.1016/j.tecto.2009.06.021

Vilà, M., Pin, C., Enrique, P., Liesa, M., 2005. Telescoping of three distinct magmatic suites in an orogenic setting: Generation of Hercynian igneous rocks of the Albera Massif (Eastern Pyrenees). Lithos 83, 97–127. https://doi.org/10.1016/j.lithos.2005.01.002

Wallace, P., Anderson, A.T., 1999. Volatiles in magmas, in: Encyclopedia of Volcanoes. pp. 149–170.

Workman, R.K., Hart, S.R., 2005. Major and trace element composition of the depleted MORB mantle (DMM). Earth Planet. Sci. Lett. 231, 53–72. https://doi.org/10.1016/J.EPSL.2004.12.005

Figure captions

Figure 1: (a) Location of the Variscan crust of the Pyrenees and main locations of Variscan granulites in Europe modified from Pin and Vielzeuf (1983). (b) Geological sketchmap of the Variscan crust of the Pyrenees and location of the studied area, modified from Cochelin et al., 2018. NPF, North Pyrenean Fault.

Figure 2: (a) Geological map of the Lesponne and the Chiroulet domes, modified from Pouget (1984) and Ternet et al (1996), with samples and cross-section locations. A. R. Aygue-Rouye sub-dome. (b) N-S geological cross-section of the Chiroulet dome. (c) NE-SW geological cross-section of the Lesponne dome.

Figure 3: Field photographs of the main magmatic rocks in the two metamorphic domes and microphotographs of the Lesponne migmatite and Chiroulet Devonian schists. (a) Contact between the diorite and the porphyritic granite in the Lesponne dome. The diorite is foliated while the porphyritic feldspars of the granite underlies the magmatic foliation. (b) Veins of porphyritic granite connected to the migmatite in the Lesponne dome. (c) Enclaves of amphibolite in the leucosome of a diatexite in the Chiroulet dome. (d) Leucogranite in the core of the Chiroulet dome showing C/S fabrics. It suggests sub-solidus deformation during its emplacement. (e) Abundance of tourmaline crystals in the Devonian schists located in the southern flank of the Chiroulet dome. (f) Stable assemblage in the Lesponne migmatite 15BL176.

Figure 4: (a) Plot of SiO_2 vs. K_2O (Middlemost, 1985; Peccerillo and Taylor, 1976). (b) Plot of A/NK vs. A/CNK (Shand, 1943). (c) REE patterns normalized to chondrite (Boynton, 1984). (d) Spider diagram of trace elements normalized to primitive mantle (McDonough and Sun, 1995). Red color is used for the intermediate to felsic peraluminous rocks and green for the mafic to intermediate metaluminous rocks. Brown symbols represent the partially molten country rocks. Black symbols are data from Debon et al., (1996). Grey diamonds in plot (b) and grey field in plot (c) represent points for a compilation of data

(Debon et al., 1996; Denèle et al., 2011; Druguet et al., 2014; Kilzi, 2014; Roberts et al., 2000; Vilà et al., 2005).

Figure 5: Plot of εNd vs. ($^{87}Sr/^{86}Sr$) ratio both corrected for an age of 300 Ma. Bulk Earth value is calculated from Workman and Hart (2005). Data from the Querigut pluton (Roberts et al., 2000) are represented by dotted fields i) dark green : mafic samples derived from a mantel source ii) light green : mafic samples cogenetic with the intermediate series iii) red : intermediate to felsic series.

Figure 6: Cathodoluminescence images of representative zircon grains from the dated samples. Blue circles and yellow circles correspond to analyses yielding Carboniferous (303 Ma) and Permian (292 Ma) ages respectively. Images correspond to sample: (a) and (b) light and dark Neouvielle granodiorites; (c), (d), (e) and (f) Lesponne diorite; (g) and (h) Lesponne granite; (i) Lesponne migmatite; (j) Chiroulet granite and (k) Chiroulet migmatite. Ages on the figure correspond to apparent $^{206}Pb/^{238}U$ ages.

Figure 7: Tera-Wasserburg representation of U-Pb analyses on zircon. For the Neouvielle pluton, dark and light ellipses represent respectively the dark and the light facies. For the metamorphic domes, yellow and blue ellipses represent the Permian and Carboniferous ages respectively. Grey ellipses are for the inherited cores and for the analyses with a recent lead loss or common lead. In the diagrams, errors ellipses and ages are reported at 2σ. All MSWD (Mean Square of the Weighted Deviates) values reported for the Concordia Ages correspond to “Concordance + Equivalence” as defined by Ludwig’s publication (1998).

Figure 8: (a) Result of phase equilibria modelling for sample 15BL176 (migmatitic micaschit of the Lesponne dome) presented as isochemical diagram section. X_{Mg} isopleths of biotite are represented. (b) Diagram showing melt fraction as a function of temperature during the cooling of a dioritic melt.

Figure 9: Schematic three-dimensional block-diagram of the studied area at 303 and 292 Ma representing the evolution of the intermediate and upper Variscan crust during the late high temperature event.

Table 1: Chemical and isotopic analyses of the samples

Location	Neouvielle		Lesponne				Chiroulet			
Rock type	granodiorite	granodiorite	diorite	granite	metatexite	micaschist	amphibolite	granite	diatexite	paragneiss
Sample name	15MSB20	15MSB22	15BL179	15BL177	15BL176	15BL180	15BL166	15BL168	15BL164	15BL169
Longitude (°)	42.84434	42.82497	42.98390	42.97511	42.97518	42.97680	42.93634	42.93882	42.94488	42.94696
Latitude (°)	0.16007	0.16706	0.14103	0.18059	0.18054	0.15370	0.12176	0.11877	0.14465	0.10938
SiO_2 / wt%	70.8	61.55	52.52	68.47	65.81	72.55	53.71	73.72	73.88	69.66
Al_2O_3	15	15.97	17.89	15.24	18.41	14.34	17.71	14.55	14.6	13.12
$Fe_2O_{3\ tot}$	2.3	5.75	7.6	3.98	6.61	3.57	9.02	1.08	0.89	5.76
MnO	0.05	0.1	0.15	0.05			0.26	0.03	0.09	
MgO	0.73	3.35	5.52	1.02	2.1	0.96	4.88	0.21	0.05	2.04
CaO	2.25	5.58	7.47	2.11	0.36	1.35	5.93	0.66	0.4	1.7
Na_2O	3.15	2.26	2.81	2.96	0.53	0.47	1.19	3.48	4.16	2.73
K_2O	3.97	2.59	2.29	3.49	3.71	3.71	3.36	4.81	4.73	2.23
TiO_2	0.27	0.68	1	0.61			0.82	0.08	/	

Cr_2O_3	0.01	0.02	0.02	0.01			0.03	0.01	0.01	
P_2O_5	0.1	0.12	0.28	0.36			0.12	0.4	0.27	
L.O.I.	1.14	1.96	2.41	1.31	1.36	1.69	2.51	0.94	0.55	1.33
Total	99.77	99.93	99.96	99.61	99.86	99.74	99.54	99.97	99.63	99.84
As / ppm	3.1	4.4	0.7	/	0.7	10.3	5.1	1.9	1.1	1.2
Ba	512.6	539.5	817.2	975.8	677.7	600.4	348.3	224.1	23.1	500.0
Be	7.1	2.0	2.2	2.0	2.9	2.0	2.3	6.4	1.1	0.8
Bi	0.2	0.0	0.1	0.1	0.3	/	0.5	1.1	0.4	0.2
Cd	0.1	0.1	0.1	0.1	0.1	0.1	2.5	0.1	0.2	0.2
Ce	53.8	45.4	78.7	122.4	91.4	98.1	46.5	11.1	4.3	55.5
Co	3.7	16.3	22.5	5.5	17.0	6.4	17.6	0.7	0.4	12.9
Cr	101.6	371.6	149.9	59.5	184.0	387.4	216.1	56.6	88.3	274.6
Cs	8.0	2.5	2.1	1.4	6.2	8.6	13.1	16.9	4.6	6.5
Cu	/	12.2	6.2	4.5	10.2	/	16.0	/	/	15.7
Dy	3.2	4.4	6.1	5.4	5.9	6.2	5.2	2.0	0.9	4.8
Er	1.5	2.5	3.3	2.5	3.2	3.7	3.3	0.8	0.6	2.6
Eu	1.0	1.0	1.9	1.9	1.4	1.3	1.2	0.3	0.1	1.4

Ga	19.4	19.2	20.1	18.7	26.8	19.5	22.9	18.0	13.6	17.2
Gd	3.7	4.4	7.0	7.0	6.5	6.1	4.4	1.4	0.4	4.8
Ge	1.7	1.4	1.8	1.6	1.8	1.7	2.4	1.7	2.7	1.5
Hf	3.3	4.8	2.9	6.8	3.8	13.3	3.1	1.7	0.3	6.4
Ho	0.6	0.9	1.2	1.0	1.2	1.3	1.2	0.4	0.2	1.0
In	0.0	0.1	0.1	0.0	0.1	0.0	0.2	0.0	/	0.1
La	26.9	21.4	31.9	67.0	47.9	48.6	22.9	5.3	2.0	25.4
Lu	0.2	0.4	0.5	0.3	0.4	0.6	0.5	0.1	0.1	0.4
Mo	4.5	19.6	2.6	2.9	4.6	13.5	9.4	3.3	4.7	8.2
Nb	9.0	9.9	8.9	12.5	13.6	17.1	7.8	9.7	0.4	10.8
Nd	21.5	21.5	43.1	50.2	40.5	41.7	20.3	4.6	1.7	25.7
Ni	11.7	90.2	47.1	7.0	43.5	28.0	21.4	9.4	12.0	34.2
Pb	40.8	12.8	10.9	38.7	24.4	13.4	306.5	23.6	25.4	13.7
Pr	5.9	5.4	10.3	13.9	10.9	11.4	5.2	1.2	0.5	6.5
Rb	163.4	92.0	77.5	83.4	150.5	125.2	284.1	199.2	138.3	96.8
Sb	0.2	0.3	0.1	/	/	0.1	0.3	/	/	/
Sm	4.5	4.8	9.1	9.2	7.9	7.8	4.4	1.3	0.5	5.5

Sn	6.4	4.1	5.4	2.5	4.8	4.5	22.6	26.1	6.6	3.6
Sr	163.0	261.9	643.4	268.0	66.3	123.9	329.5	56.6	22.7	213.4
Ta	1.7	0.9	1.0	1.0	1.4	1.5	0.7	2.7	0.1	1.2
Tb	0.6	0.7	1.0	1.0	1.0	1.0	0.8	0.3	0.1	0.8
Th	13.2	9.2	9.9	36.2	14.6	16.8	6.3	1.5	0.7	6.9
Tm	0.2	0.4	0.5	0.3	0.4	0.6	0.5	0.1	0.1	0.4
U	3.6	3.5	3.9	3.7	3.4	3.9	2.3	2.4	1.5	2.9
V	16.9	78.6	184.4	41.3	87.7	99.9	198.1	2.3	1.8	106.6
W	4.5	7.1	1.7	3.0	6.1	16.6	13.1	5.1	3.9	9.6
Y	16.8	25.2	33.2	26.1	31.4	35.1	31.1	10.8	6.4	26.0
Yb	1.5	2.4	3.2	2.1	3.0	3.8	3.4	0.5	0.9	2.5
Zn	43.5	81.8	74.0	45.9	134.7	62.9	646.7	38.0	9.7	84.7
Zr	103.9	173.3	96.6	245.3	134.4	500.5	112.9	44.8	4.8	240.5
La/Yb	18.0	8.9	10.0	31.5	16.0	12.7	6.7	9.8	2.2	10.3
Nb/Ta	5.3	10.6	9.0	12.7	9.5	11.1	11.9	3.6	3.8	9.2
$^{87}Rb/^{86}Sr$	2.828149685	0.990460788	0.339488811	0.877464331	6.402138191	2.850307291	2.4309565	9.917365977	17.16784924	1.279104993
$^{87}Sr/^{86}Sr$ (err. 2σ)	0.725613 (14)	0.714813 (20)	0.707447 (6)	0.715559 (12)	0.746276 (14)	0.729244 (18)	0.712902 (10)	0.757092 (14)	0.784814 (12)	0.714694 (22)

$(^{87}Sr/^{86}Sr)_{300Ma}$	0.713539384	0.710584637	0.705997693	0.711813029	0.718944717	0.717075791	0.702524036	0.714753905	0.711522963	0.70923339
$^{147}Sm/^{144}Nd$	0.132430604	0.139548605	0.132222424	0.114921185	0.122483087	0.117132853	0.136062037	0.18214844	0.176900693	0.133172574
$^{143}Nd/^{144}Nd$ (err.2σ)	0.512084 (5)	0.512101 (4)	0.512391 (6)	0.512169 (5)	0.512012 (4)	0.511923 (4)	0.512279 (11)	0.512248 (9)	0.511955 (15)	0.512317 (5)
$\varepsilon_{Nd\ 300Ma}$	-8.221736757	-8.162765494	-2.220530139	-5.891070998	-9.245930349	-10.77825425	-4.554192731	-6.926305049	-12.44502702	-3.7015795

Table 2: LA-ICPMS data for zircons. % Conc = percentage of concordance calculated as 100 × ($^{206}Pb/^{238}U$Age) / ($^{207}Pb/^{235}U$Age).

	Content (ppm)				Isotope ratios				Ages (Ma)						
Zircon	Pb	U	Th	Th/U	$^{238}U/^{206}Pb$	1 σ (%)	$^{207}Pb/^{206}Pb$	1 σ (%)	$^{207}Pb/^{235}U$	1 σ	$^{206}Pb/^{238}U$	1 σ	$^{207}Pb/^{206}Pb$	1 σ	%Conc.
15MSB20 (Neouvielle granodiorite)															
6160117a	43	938	113	0.12	20.5	1.5	0.0519	1.2	303	4	307	4	280	24	101
7160117a	12	244	90	0.37	20.6	1.5	0.0528	1.3	307	4	305	4	320	26	99
8160117a	29	605	133	0.22	20.6	1.5	0.0528	1.2	307	4	305	4	321	24	99
9160117a	12	250	85	0.34	20.4	1.5	0.0521	1.3	306	4	308	4	290	25	101
10160117a	41	816	367	0.45	20.5	1.5	0.0521	1.2	305	4	307	4	291	24	101
1116011	13	260	81	0.3	20.6	1.5	0.0520	1.3	304	4	306	4	287	26	101

7a				1											
12160117a	14	289	98	0.34	20.6	1.5	0.0524	1.3	306	4	306	4	304	25	100
23160117a	12	234	80	0.34	20.7	1.5	0.0523	1.3	303	4	304	4	297	26	100
27160117a	47	981	284	0.29	20.9	1.5	0.0523	1.2	301	4	302	4	300	24	100
28160117a	50	1065	213	0.2	20.7	1.5	0.0523	1.2	303	4	304	4	298	24	100
31160117a	15	299	135	0.45	20.7	1.5	0.0528	1.3	306	4	305	4	318	27	100
33160117a	47	949	332	0.35	20.7	1.5	0.0527	1.2	306	4	305	4	318	24	100
34160117a	17	334	134	0.4	20.8	1.5	0.0526	1.3	304	4	303	4	313	26	100
22200117c	65	1394	293	0.21	20.7	1.4	0.0527	1.5	305	3	304	4	314	25	100
23200117c	15	297	119	0.4	20.6	1.4	0.0520	1.6	303	4	305	4	285	28	101
3120011	30	624	193	0.3	20.7	1.4	0.0519	1.7	302	4	305	4	282	31	101

7c				1											
34200117c	19	380	144	0.38	20.8	1.4	0.0524	1.6	303	4	303	4	304	28	100
15MSB22 (Neouvielle granodiorite)															
6160117c	13	252	83	0.33	20.7	1.4	0.0520	1.3	302	4	305	4	284	26	101
10160117c	11	213	75	0.35	20.7	1.5	0.0525	1.3	304	4	304	4	306	26	100
11160117c	15	304	97	0.32	20.9	1.5	0.0526	1.3	302	4	301	4	311	25	100
17160117c	14	285	80	0.28	20.8	1.5	0.0526	1.3	304	4	303	4	313	25	100
18160117c	16	320	115	0.36	20.7	1.5	0.0517	1.3	300	4	304	4	270	25	101
19160117c	11	223	65	0.29	20.8	1.5	0.0533	1.3	307	4	303	4	340	26	99
30160117c	9	192	63	0.33	20.7	1.5	0.0530	1.3	308	4	305	4	330	27	99
3116011	11	219	79	0.3	20.6	1.5	0.0520	1.3	302	4	305	4	283	27	101

7c				6											
32160117c	12	246	81	0.33	20.9	1.5	0.0521	1.3	299	4	301	4	289	27	101
34160117c	14	274	118	0.43	20.7	1.5	0.0522	1.3	303	4	305	4	292	27	101
5200117d	28	572	246	0.43	20.8	1.4	0.0525	1.5	303	3	302	4	305	26	100
6200117d	16	334	154	0.46	21.0	1.4	0.0523	1.5	299	3	300	4	296	27	100
7200117d	14	298	101	0.34	20.9	1.4	0.0518	1.5	298	4	301	4	276	28	101
9200117d	20	408	180	0.44	20.9	1.4	0.0529	1.6	303	4	301	4	323	28	99
10200117d	21	428	163	0.38	20.9	1.4	0.0522	1.5	301	3	301	4	296	27	100
18200117d	9	180	58	0.32	21.1	1.4	0.0521	1.7	297	4	298	4	287	33	100
15BL179 (Lesponne diorite)															
5160117e	48	926	556	0.6	20.8	1.5	0.0525	1.2	303	4	303	4	308	24	100

6160117e	26	434	486	1.12	20.9	1.5	0.0530	1.2	304	4	301	4	328	24	99
7160117e	44	786	676	0.86	20.7	1.5	0.0525	1.2	304	4	304	4	309	24	100
8160117e	57	1002	862	0.86	20.6	1.5	0.0527	1.2	307	3	306	4	315	23	100
9160117e	16	307	181	0.59	20.7	1.5	0.0522	1.2	303	4	304	4	292	25	100
10160117e	59	1145	641	0.56	21.0	1.5	0.0528	1.2	303	3	300	4	321	23	99
11160117e	50	1007	594	0.59	21.9	1.5	0.0528	1.2	292	3	288	4	319	23	99
12160117e	38	661	641	0.97	21.0	1.5	0.0525	1.2	301	3	300	4	306	24	100
16160117e	39	774	426	0.55	21.7	1.5	0.0525	1.2	292	3	291	4	307	24	100
17160117e	37	612	667	1.09	20.8	1.5	0.0530	1.2	306	4	303	4	330	24	99
18160117e	49	831	897	1.08	20.9	1.5	0.0523	1.2	300	3	301	4	297	24	100

19160117e	65	1119	1287	1.15	21.7	1.5	0.0522	1.2	291	3	290	4	293	24	100
20160117e	30	599	365	0.61	21.9	1.5	0.0523	1.2	289	3	288	4	300	24	100
21160117e	26	591	142	0.24	22.5	1.5	0.0533	1.2	287	3	281	4	342	24	98
22160117e	41	759	486	0.64	20.8	1.5	0.0528	1.2	305	4	303	4	322	24	99
23160117e	33	562	652	1.16	21.6	1.5	0.0527	1.2	294	3	291	4	315	24	99
27160117e	35	579	758	1.31	21.8	1.5	0.0532	1.3	294	3	289	4	335	25	98
29160117e	23	405	409	1.01	21.1	1.5	0.0530	1.3	302	4	299	4	328	26	99
30160117e	18	376	165	0.44	22.3	1.5	0.0533	1.3	290	3	283	4	340	25	98
31160117e	30	626	269	0.43	21.6	1.5	0.0528	1.2	294	3	291	4	318	25	99
32160117e	47	1085	54	0.05	21.8	1.5	0.0521	1.2	290	3	290	4	291	24	100

33160117e	36	632	689	1.09	21.7	1.5	0.0523	1.2	292	3	291	4	297	25	100
34160117e	24	501	180	0.36	21.6	1.5	0.0522	1.3	292	3	292	4	292	25	100
6200117b	28	525	630	1.2	23.5	1.3	0.0519	1.5	270	3	269	3	281	26	100
8200117b	64	1407	788	0.56	24.0	1.3	0.0519	1.4	265	3	263	3	283	24	99
9200117b	71	1601	801	0.5	24.1	1.3	0.0524	1.4	266	3	262	3	303	24	98
11200117b	25	506	390	0.77	23.0	1.3	0.0526	1.5	278	3	274	3	312	25	99
16200117b	103	1755	2404	1.37	22.5	1.3	0.0531	1.4	286	3	280	3	331	24	98
17200117b	73	1429	1300	0.91	23.6	1.3	0.0532	1.4	275	3	268	3	338	24	97
18200117b	43	887	470	0.53	22.0	1.3	0.0534	1.5	293	3	286	3	345	25	98
19200117b	65	1300	1105	0.85	23.4	1.4	0.0526	1.4	274	3	269	3	312	24	98

20200117b	32	613	570	0.93	22.5	1.3	0.0522	1.5	281	3	280	3	292	25	100
21200117b	34	686	370	0.54	22.0	1.3	0.0537	1.5	294	3	286	3	356	25	97
22200117b	74	1459	1269	0.87	23.2	1.3	0.0524	1.5	276	3	273	3	301	24	99
23200117b	41	809	720	0.89	23.2	1.3	0.0524	1.5	275	3	272	3	302	25	99
28200117b	19	450	108	0.24	22.8	1.3	0.0526	1.5	281	3	277	3	313	26	99
29200117b	72	1291	1239	0.96	21.4	1.4	0.0521	1.5	294	3	295	3	288	25	100
30200117b	19	334	291	0.87	20.5	1.3	0.0524	1.5	306	4	307	4	303	27	100
31200117b	44	866	520	0.6	21.5	1.4	0.0523	1.5	294	3	293	3	297	26	100
32200117b	65	1138	1343	1.18	21.6	1.4	0.0523	1.5	293	3	292	3	297	26	100
33200117b	56	1020	908	0.89	21.3	1.4	0.0525	1.5	297	3	296	3	309	26	100

34200117b	53	872	1125	1.29	21.3	1.3	0.0525	1.5	297	3	296	3	305	26	100
15BL177 (Lesponne granite)															
6160117d	51	924	942	1.02	22.0	1.5	0.0527	1.2	290	3	287	4	315	24	99
7160117d	33	649	441	0.68	21.9	1.5	0.0534	1.2	294	3	288	4	344	24	98
8160117d	*52*	*729*	350	*0.48*	*14.8*	*1.5*	*0.0566*	*1.2*	*430*	*5*	*422*	*5*	*474*	*23*	*98*
9160117d	53	919	1075	1.17	22.0	1.5	0.0527	1.2	290	3	286	4	317	24	99
10160117d	59	1296	467	0.36	22.7	1.5	0.0572	1.2	303	3	278	4	500	23	92
11160117d	21	384	388	1.01	21.9	1.5	0.0531	1.2	292	4	288	4	332	25	99
12160117d	57	1286	231	0.18	21.8	1.5	0.0524	1.2	290	3	289	4	302	24	100
16160117d	*13*	*118*	65	*0.55*	*9.4*	*1.5*	*0.0616*	*1.3*	*653*	*7*	*650*	*8*	*661*	*24*	*100*
1716011	54	1044	762	0.7	21.9	1.5	0.0523	1.2	289	3	288	4	296	24	100

7d				3											
18160117d	49	848	890	1.05	21.5	1.5	0.0531	1.2	298	3	293	4	334	24	98
19160117d	34	735	250	0.34	21.9	1.5	0.0527	1.2	290	3	287	4	314	24	99
20160117d	*26*	*261*	204	*0.78*	*11.5*	*1.5*	*0.0592*	*1.2*	*543*	*6*	*536*	*7*	*573*	*23*	*99*
22160117d	26	580	191	0.33	22.5	1.5	0.0543	1.2	292	3	281	4	384	24	96
27160117d	*64*	*725*	44	*0.06*	*10.6*	*1.5*	*0.0600*	*1.2*	*584*	*6*	*579*	*7*	*603*	*23*	*99*
28160117d	*29*	*275*	85	*0.31*	*9.5*	*1.5*	*0.0615*	*1.2*	*649*	*7*	*647*	*8*	*657*	*23*	*100*
29160117d	*17*	*215*	65	*0.3*	*13.2*	*1.5*	*0.0577*	*1.3*	*479*	*5*	*470*	*6*	*518*	*24*	*98*
30160117d	135	2283	3036	1.33	22.1	1.5	0.0542	1.2	295	3	285	4	379	24	97
31160117d	*75*	*965*	154	*0.16*	*12.3*	*1.5*	*0.0581*	*1.2*	*507*	*5*	*502*	*6*	*531*	*24*	*99*
3216011	*13*	*1489*	253	*0.1*	*10.4*	*1.5*	*0.0602*	*1.2*	*594*	*6*	*590*	*7*	*611*	*23*	*99*

7d	*8*			*7*											
5180117g	70	1437	374	0.26	20.2	1.4	0.0543	1.3	319	3	311	4	381	24	97
6180117g	79	1931	309	0.16	23.7	1.4	0.0525	1.3	271	3	267	3	308	24	99
7180117g	34	895	9	0.01	24.4	1.4	0.0530	1.3	266	3	259	3	330	25	97
8180117g	70	1282	1128	0.88	21.6	1.4	0.0527	1.3	294	3	292	3	317	25	99
9180117g	60	1553	47	0.03	24.1	1.4	0.0537	1.3	272	3	262	3	357	24	96
10180117g	30	597	376	0.63	21.6	1.4	0.0546	1.3	304	3	292	3	396	25	96
11180117g	85	1867	411	0.22	21.6	1.4	0.0559	1.3	310	3	292	3	447	23	94
12180117g	81	2062	186	0.09	24.3	1.4	0.0543	1.3	273	3	261	3	381	24	96
16180117g	40	852	588	0.69	23.3	1.4	0.0528	1.3	276	3	271	3	321	26	98
1718011	61	1587	365	0.2	25.4	1.4	0.0534	1.3	259	3	249	3	346	25	96

7g				3												
18180117g	43	844	734	0.87	23.3	1.4	0.0530	1.3	277	3	271	3	328	26	98
19180117g	65	1398	979	0.7	23.9	1.4	0.0531	1.3	271	3	264	3	332	25	97
20180117g	39	745	738	0.99	22.9	1.4	0.0543	1.4	287	3	276	3	382	26	96
21180117g	54	1230	467	0.38	23.3	1.4	0.0537	1.4	280	3	271	3	356	27	97
22180117g	57	1439	29	0.02	23.1	1.4	0.0521	1.3	275	3	273	3	290	26	99
23180117g	78	1656	1225	0.74	23.8	1.4	0.0526	1.4	270	3	265	3	312	26	98
6200117e	26	352	67	0.19	14.0	1.3	0.0612	1.5	478	5	443	5	645	24	93
7200117e	*38*	*377*	102	*0.27*	*10.1*	*1.3*	*0.0625*	*1.5*	*624*	*6*	*606*	*7*	*690*	*23*	*97*
8200117e	*53*	*441*	578	*1.31*	*11.1*	*1.3*	*0.0614*	*1.4*	*576*	*5*	*557*	*6*	*653*	*23*	*97*
9200117	*23*	*214*	158	*0.7*	*10.8*	*1.3*	*0.0636*	*1.5*	*604*	*6*	*571*	*6*	*728*	*24*	*95*

e				*4*											
10200117e	49	944	1038	1.1	24.3	1.3	0.0532	1.5	268	3	260	3	338	24	97
11200117e	82	1518	1670	1.1	23.4	1.3	0.0525	1.4	274	3	270	3	308	24	99
12200117e	29	577	467	0.81	23.5	1.3	0.0529	1.5	274	3	269	3	323	25	98
16200117e	124	2412	2629	1.09	24.2	1.3	0.0523	1.4	265	3	261	3	299	24	98
17200117e	19	343	367	1.07	22.0	1.3	0.0531	1.6	292	3	287	3	334	28	98
18200117e	93	2107	1138	0.54	24.3	1.3	0.0526	1.4	265	3	260	3	313	24	98
19200117e	123	2260	1876	0.83	21.6	1.3	0.0523	1.4	293	3	292	3	298	24	100
20200117e	62	1384	623	0.45	23.5	1.3	0.0527	1.5	274	3	269	3	316	25	98
21200117e	73	1393	1212	0.87	22.3	1.3	0.0538	1.5	291	3	283	3	363	25	97
2220011	24	471	396	0.8	23.0	1.4	0.0536	1.5	282	3	274	3	353	26	97

7e				4											
23200117e	*38*	*388*	109	*0.28*	*10.2*	*1.3*	*0.0603*	*1.5*	*604*	*6*	*601*	*7*	*615*	*24*	*100*
27200117e	29	554	465	0.84	21.8	1.4	0.0520	1.6	289	3	290	3	285	28	100
28200117e	13	285	83	0.29	20.8	1.4	0.0540	1.6	310	4	302	3	371	28	97
29200117e	76	1652	611	0.37	21.9	1.4	0.0520	1.5	287	3	288	3	285	26	100
30200117e	23	387	395	1.02	20.4	1.4	0.0595	1.5	343	4	308	4	587	25	90
31200117e	38	816	318	0.39	21.7	1.3	0.0524	1.5	292	3	290	3	301	26	99
32200117e	43	984	384	0.39	23.4	1.4	0.0560	1.5	289	3	270	3	450	25	93
33200117e	33	587	628	1.07	21.5	1.4	0.0519	1.5	291	3	293	3	280	27	101
34200117e	84	1777	1564	0.88	23.7	1.4	0.0526	1.5	271	3	267	3	311	26	99
15BL176 (Lesponne migmatite)															

5190117b	42	900	90	0.1	20.8	1.5	0.0564	1.3	322	4	303	4	467	24	94
6190117b	104	2391	120	0.05	21.4	1.5	0.0528	1.3	298	3	295	4	320	24	99
7190117b	61	1074	967	0.9	20.6	1.5	0.0525	1.3	306	3	306	4	307	24	100
8190117b	98	2176	370	0.17	21.6	1.5	0.0548	1.3	305	3	292	3	405	23	96
9190117b	155	3333	1367	0.41	22.4	1.5	0.0564	1.2	303	3	282	3	466	23	93
10190117b	*73*	*1069*	118	*0.11*	*14.1*	*1.5*	*0.0768*	*1.3*	*568*	*5*	*441*	*5*	*1115*	*21*	*78*
11190117b	92	2104	0	0	20.8	1.5	0.0531	1.3	306	3	303	4	332	24	99
16190117b	59	1250	288	0.23	20.8	1.5	0.0535	1.3	308	3	302	4	350	25	98
17190117b	73	1598	176	0.11	20.8	1.5	0.0533	1.3	307	3	303	4	343	24	99
18190117b	*57*	*625*	194	*0.31*	*11.0*	*1.5*	*0.0588*	*1.3*	*560*	*6*	*561*	*7*	*558*	*23*	*100*

19190117b	*49*	*404*	*473*	*1.17*	*10.7*	*1.5*	*0.0597*	*1.3*	*580*	*6*	*576*	*7*	*594*	*24*	*99*
20190117b	115	2744	357	0.13	22.7	1.5	0.0537	1.3	286	3	278	3	357	24	97
21190117b	24	423	372	0.88	20.9	1.5	0.0527	1.4	303	4	301	4	316	28	99
22190117b	102	2000	1040	0.52	21.0	1.5	0.0532	1.3	304	3	300	4	335	25	99
23190117b	44	832	83	0.1	18.0	1.5	0.0560	1.3	363	4	349	4	452	24	96
27190117b	75	1535	553	0.36	20.7	1.5	0.0521	1.3	303	3	305	4	290	25	101
28190117b	84	1818	218	0.12	20.7	1.5	0.0521	1.3	303	3	305	4	288	25	101
30190117b	*16*	*149*	113	*0.76*	*10.7*	*1.5*	*0.0600*	*1.4*	*583*	*6*	*577*	*7*	*604*	*27*	*99*
31190117b	70	1800	90	0.05	24.0	1.5	0.0541	1.3	275	3	263	3	374	25	96
32190117b	110	2641	264	0.1	22.7	1.5	0.0522	1.3	280	3	279	3	293	25	100

33190117b	94	2214	221	0.1	22.4	1.5	0.0528	1.3	286	3	282	3	320	25	99
34190117b	103	2200	418	0.19	20.7	1.5	0.0522	1.3	303	3	304	4	295	26	100
5200117a	24	448	493	1.1	22.4	1.4	0.0524	1.5	283	3	281	3	303	25	99
7200117a	*20*	*228*	64	*0.28*	*11.1*	*1.4*	*0.0592*	*1.5*	*559*	*6*	*556*	*6*	*574*	*24*	*99*
8200117a	60	1496	15	0.01	22.4	1.4	0.0526	1.4	285	3	282	3	312	24	99
10200117a	9	180	112	0.62	21.3	1.4	0.0529	1.6	299	4	296	4	325	29	99
11200117a	*118*	*1025*	390	*0.38*	*8.9*	*1.4*	*0.0626*	*1.4*	*690*	*6*	*689*	*8*	*695*	*22*	*100*
12200117a	154	2954	30	0.01	17.6	1.4	0.0558	1.4	368	4	356	4	444	22	97
16200117a	*245*	*2443*	366	*0.15*	*9.6*	*1.4*	*0.0640*	*1.4*	*662*	*6*	*639*	*7*	*743*	*22*	*97*
18200117a	102	1897	2087	1.1	23.1	1.4	0.0555	1.4	291	3	274	3	431	23	94

19200117a	20	475	133	0.28	23.6	1.4	0.0528	1.5	273	3	268	3	321	25	98
20200117a	*50*	*577*	63	*0.11*	*11.1*	*1.4*	*0.0632*	*1.4*	*587*	*6*	*554*	*6*	*714*	*23*	*94*
21200117a	82	2050	287	0.14	23.9	1.4	0.0525	1.4	269	3	265	3	308	24	99
22200117a	103	2049	1721	0.84	23.4	1.4	0.0524	1.4	273	3	269	3	302	24	99
23200117a	36	657	696	1.06	22.3	1.4	0.0544	1.5	294	3	283	3	389	25	96
27200117a	84	1848	869	0.47	23.1	1.4	0.0538	1.4	282	3	273	3	361	24	97
29200117a	*16*	*162*	50	*0.31*	*10.2*	*1.4*	*0.0620*	*1.5*	*619*	*6*	*604*	*7*	*673*	*25*	*98*
31200117a	41	1007	40	0.04	23.3	1.4	0.0566	1.5	294	3	272	3	477	25	93
32200117a	16	378	110	0.29	23.4	1.3	0.0528	1.5	275	3	270	3	321	27	98
34200117a	*31*	*281*	219	*0.78*	*10.5*	*1.4*	*0.0595*	*1.5*	*585*	*6*	*586*	*7*	*584*	*25*	*100*

15BL168 (Chiroulet granite)															
5170117f	7	59	65	1.11	10.1	1.3	0.0615	1.4	620	7	609	7	658	28	98
6170117f	169	2204	419	0.19	12.7	1.3	0.0577	1.1	494	5	489	6	517	22	99
7170117f	441	11248	112	0.01	23.5	1.3	0.0553	1.1	285	3	269	3	426	23	94
8170117f	28	301	27	0.09	10.5	1.3	0.0665	1.2	638	6	587	7	822	23	92
9170117f	61	383	234	0.61	7.0	1.3	0.0702	1.2	881	7	860	10	934	22	98
10170117f	49	438	337	0.77	10.2	1.3	0.0602	1.2	603	6	601	7	609	23	100
11170117f	228	6340	63	0.01	25.4	1.3	0.0530	1.1	256	3	249	3	329	23	97
17170117f	60	1414	14	0.01	21.5	1.3	0.0533	1.2	299	3	294	3	341	24	98
18170117f	107	1923	77	0.04	16.8	1.3	0.0575	1.2	393	4	373	4	512	23	95
1917011	15	214	19	0.0	13.3	1.3	0.0580	1.3	479	5	468	5	531	27	98

7f				9											
21170117f	152	1207	616	0.51	8.8	1.3	0.0702	1.2	752	7	692	8	935	22	92
22170117f	23	542	11	0.02	21.6	1.3	0.0531	1.2	297	3	292	3	332	26	98
23170117f	82	2085	0	0	23.4	1.3	0.0546	1.2	283	3	270	3	397	24	95
27170117f	127	2938	59	0.02	21.3	1.3	0.0532	1.2	300	3	295	3	337	24	98
28170117f	161	3828	38	0.01	21.6	1.3	0.0526	1.2	294	3	291	3	312	25	99
30170117f	54	1177	24	0.02	20.1	1.3	0.0553	1.2	327	4	313	4	424	25	96
31170117f	274	7304	73	0.01	24.3	1.3	0.0528	1.2	266	3	260	3	321	25	98
32170117f	160	3121	250	0.08	18.7	1.3	0.0568	1.2	355	4	336	4	485	24	95
33170117f	90	2078	42	0.02	21.3	1.3	0.0562	1.2	315	3	295	3	459	25	94
3417011	38	905	0	0	21.6	1.3	0.0527	1.3	294	3	291	3	314	27	99

7f															
6170117g	764	17902	179	0.01	21.6	1.3	0.0546	1.1	303	3	291	3	397	23	96
7170117g	43	362	235	0.65	9.4	1.3	0.0619	1.2	658	6	654	7	672	23	99
8170117g	60	1401	0	0	21.3	1.3	0.0520	1.2	295	3	296	3	287	24	100
9170117g	121	926	148	0.16	7.4	1.3	0.0689	1.1	836	7	814	9	895	21	97
11170117g	104	2008	120	0.06	18.4	1.3	0.0556	1.1	354	4	341	4	435	23	96
16170117g	80	962	144	0.15	11.6	1.3	0.0583	1.2	536	5	535	6	541	24	100
17170117g	99	932	550	0.59	10.3	1.3	0.0611	1.2	605	6	595	7	642	23	98
18170117g	44	363	87	0.24	8.2	1.3	0.0645	1.2	748	7	744	8	759	23	99
19170117g	50	546	180	0.33	11.1	1.3	0.0586	1.2	554	5	554	6	553	24	100
2017011	85	2036	0	0	21.8	1.3	0.0529	1.2	293	3	289	3	324	24	99

7g															
21170117g	112	1349	13	0.01	11.0	1.3	0.0614	1.2	578	5	560	6	652	23	97
22170117g	140	3546	35	0.01	23.2	1.3	0.0536	1.2	281	3	272	3	354	24	97
23170117g	27	244	273	1.12	11.2	1.3	0.0585	1.2	550	6	551	6	549	25	100
27170117g	85	825	198	0.24	9.5	1.3	0.0618	1.2	649	6	644	7	667	23	99
28170117g	55	1107	33	0.03	19.5	1.3	0.0657	1.2	388	4	323	4	796	23	83
29170117g	22	247	96	0.39	11.8	1.3	0.0584	1.3	530	6	526	6	545	26	99
30170117g	31	285	63	0.22	9.1	1.3	0.0628	1.2	679	7	673	8	700	24	99
31170117g	161	1621	324	0.2	9.9	1.3	0.0644	1.2	651	6	622	7	753	23	96
32170117g	129	3172	32	0.01	22.4	1.3	0.0522	1.2	283	3	282	3	294	25	100
3317011	12	2372	24	0.0	17.4	1.3	0.0627	1.2	410	4	361	4	697	24	88

7g	6			1											
3417011 7g	18 3	4701	47	0.0 1	23.4	1.3	0.0561	1.2	290	3	270	3	456	24	93
5180117 e	33	371	100	0.2 7	11.1	1.4	0.0598	1.3	563	5	555	6	596	23	99
6180117 e	51	1097	121	0.1 1	21.3	1.4	0.0555	1.3	312	3	296	3	431	24	95
7180117 e	14 5	4088	41	0.0 1	25.6	1.4	0.0531	1.3	256	3	247	3	334	24	96
8180117 e	72	870	78	0.0 9	11.6	1.4	0.0602	1.3	549	5	534	6	612	23	97
9180117 e	52	735	74	0.1	13.2	1.4	0.0584	1.3	482	5	469	5	544	23	97
1018011 7e	43	199	378	1.9	7.0	1.4	0.0724	1.3	904	7	866	10	997	22	96
1118011 7e	63	1724	0	0	25.3	1.3	0.0561	1.3	271	3	250	3	455	23	92
1218011 7e	58	871	17	0.0 2	13.9	1.4	0.0609	1.3	480	5	448	5	637	23	93
1618011	83	2017	20	0.0	22.1	1.4	0.0522	1.3	287	3	286	3	296	24	100

7e				1											
18180117e	247	6422	64	0.01	23.9	1.4	0.0548	1.3	279	3	264	3	405	23	95
19180117e	23	172	170	0.99	9.2	1.4	0.0690	1.5	721	7	666	8	897	26	92
20180117e	52	289	205	0.71	6.2	1.4	0.0731	1.3	976	8	958	10	1016	22	98
21180117e	127	3395	34	0.01	24.5	1.4	0.0530	1.3	265	3	258	3	328	24	97
22180117e	118	2765	221	0.08	22.7	1.4	0.0533	1.3	285	3	279	3	341	24	98
23180117e	134	3646	36	0.01	24.9	1.4	0.0520	1.3	258	3	254	3	287	24	98
27180117e	174	4552	46	0.01	24.0	1.4	0.0523	1.3	267	3	264	3	298	25	99
29180117e	19	111	92	0.83	7.0	1.4	0.0701	1.4	882	8	863	9	931	24	98
30180117e	134	3668	37	0.01	25.2	1.3	0.0526	1.3	257	3	251	3	312	25	98
3118011	57	448	13	0.0	7.4	1.4	0.0692	1.3	841	7	818	9	904	23	97

7e				*3*											
32180117e	*7*	*66*	*30*	*0.46*	*9.7*	*1.4*	*0.0629*	*1.6*	*647*	*7*	*631*	*7*	*704*	*30*	*98*
33180117e	35	811	*24*	0.03	21.8	1.4	0.0533	1.4	295	3	290	3	340	26	98
34180117e	153	3731	*75*	0.02	22.5	1.4	0.0523	1.3	282	3	280	3	300	25	99
15BL164 (Chiroulet migmatite)															
81801177a	232	5530	12	0	21.6	1.4	0.0527	1.3	294	3	292	3	316	24	99
10180117a	79	2148	2	0	24.7	1.4	0.0532	1.3	264	3	256	3	336	24	97
12180117a	366	9724	9	0	24.1	1.4	0.0528	1.3	268	3	262	3	320	24	98
16180117a	190	4690	3	0	22.5	1.4	0.0528	1.3	285	3	280	3	321	24	98
17180117a	218	5219	3	0	21.9	1.4	0.0532	1.3	294	3	288	3	338	24	98
18180117a	196	4900	4	0	22.7	1.4	0.0527	1.3	282	3	278	3	315	24	99

19180117a	326	7827	10	0	21.9	1.4	0.0527	1.3	291	3	288	3	314	24	99
22180117a	350	8187	9	0	21.4	1.4	0.0535	1.3	300	3	294	3	350	24	98
29180117a	310	7414	8	0	21.9	1.4	0.0527	1.3	291	3	288	3	318	24	99
30180117a	330	8742	74	0.01	24.4	1.4	0.0529	1.3	266	3	259	3	323	25	97
32180117a	465	10744	30	0	21.2	1.4	0.0525	1.3	298	3	297	3	306	25	100
34180117a	222	5223	6	0	21.6	1.4	0.0530	1.3	297	3	292	3	331	25	98
6180117d	158	3748	7	0	21.2	1.4	0.0529	1.3	300	3	297	4	324	24	99
7180117d	157	3934	4	0	22.5	1.4	0.0531	1.3	286	3	281	3	333	24	98
9180117d	215	5493	6	0	22.9	1.4	0.0521	1.3	277	3	275	3	292	24	99
12180117d	442	11315	6	0	23.1	1.4	0.0523	1.3	276	3	273	3	299	24	99

17180117d	705	17095	413	0.02	22.2	1.4	0.0521	1.3	285	3	284	3	291	24	100
18180117d	187	4785	9	0	23.4	1.4	0.0529	1.3	275	3	270	3	323	25	98
19180117d	146	3660	4	0	23.0	1.4	0.0531	1.3	280	3	274	3	331	25	98
20180117d	306	8061	7	0	24.2	1.4	0.0529	1.3	268	3	261	3	323	25	97
27180117d	495	12114	33	0	22.7	1.3	0.0522	1.3	279	3	278	3	294	26	100
30180117d	201	4917	5	0	22.9	1.3	0.0529	1.3	280	3	275	3	325	26	98
31180117d	250	6163	11	0	23.1	1.3	0.0530	1.4	279	3	273	3	329	26	98
33180117d	193	4848	4	0	23.6	1.3	0.0524	1.4	272	3	268	3	304	27	99
34180117d	213	5242	5	0	23.1	1.3	0.0529	1.4	278	3	273	3	325	27	98

Appendix A: Analytical method for XRF measurements.

Appendix B: Operating conditions for the LA-ICPMS equipment and Plesovice analyses for quality control.

Appendix C: Solid solution models used for phase equilibria modelling.

Highlights

- Variscan Pyrenees were affected by a late orogenic high temperature event.
- Late Variscan magmatism lasted from ca. 303 Ma to ca. 290 Ma in the Pyrenees.
- The intermediate crust of the Pyrenees remained partially molten for about 10 My.
- Both mantle and crustal magma sources were evidenced in the Pyrenees.
- Magmatism acted as an external heat source for crustal heating.

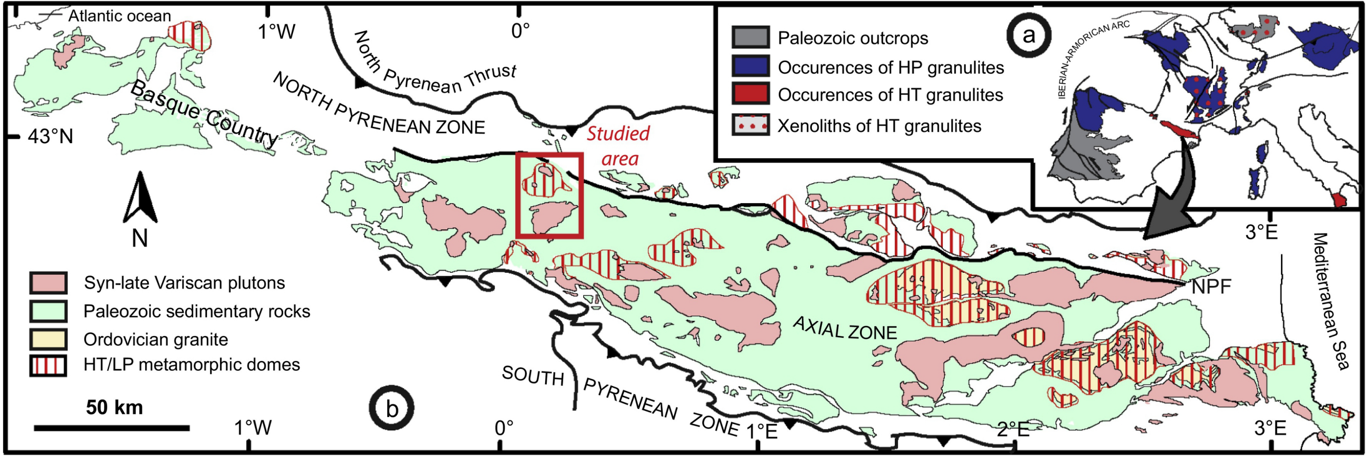
Atlantic ocean
1°W
0°
North Pyrenean Thrust
NORTH PYRENEAN ZONE
Basque Country
43°N
N
Studied area
Paleozoic outcrops
Occurences of HP granulites
Occurences of HT granulites
Xenoliths of HT granulites
a
IBERIAN-ARMORICAN ARC
3°E
Mediterranean Sea
NPF
AXIAL ZONE
Syn-late Variscan plutons
Paleozoic sedimentary rocks
Ordovician granite
HT/LP metamorphic domes
50 km
b
1°W
0°
SOUTH PYRENEAN ZONE
1°E
2°E
3°E

Figure 1

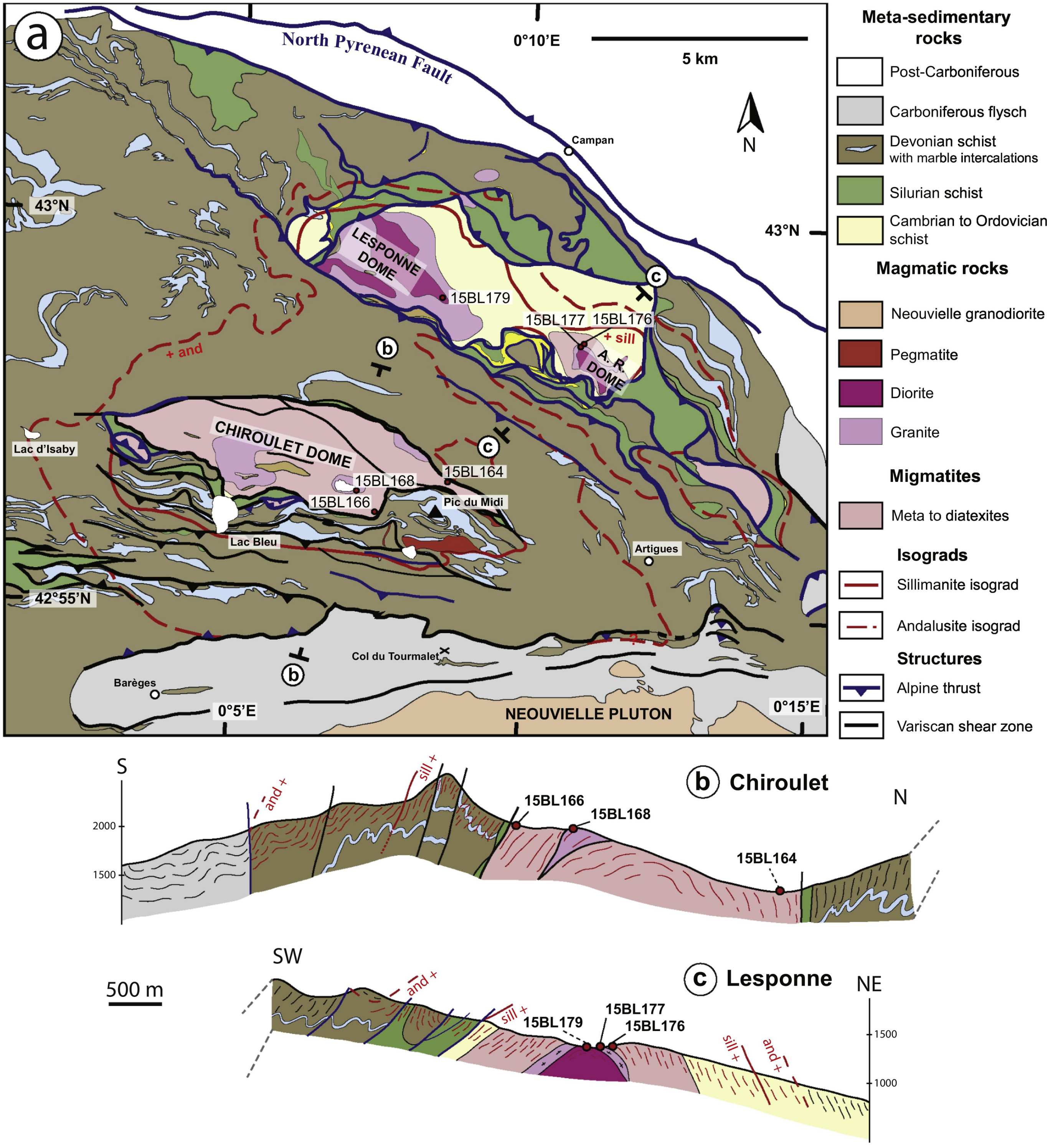

a
North Pyrenean Fault
0°10'E
5 km
N
Campan
43°N
43°N
LESPONNE DOME
15BL179
15BL177
15BL176
+ sill
A. R. DOME
+ and
b
c
c
CHIROULET DOME
Lac d'Isaby
15BL168
15BL164
15BL166
Pic du Midi
Lac Bleu
Artigues
42°55'N
Col du Tourmalet
b
Barèges
0°5'E
NEOUVIELLE PLUTON
0°15'E
Meta-sedimentary rocks
Post-Carboniferous
Carboniferous flysch
Devonian schist with marble intercalations
Silurian schist
Cambrian to Ordovician schist
Magmatic rocks
Neouvielle granodiorite
Pegmatite
Diorite
Granite
Migmatites
Meta to diatexites
Isograds
Sillimanite isograd
Andalusite isograd
Structures
Alpine thrust
Variscan shear zone
S
b Chiroulet
N
and +
sill +
15BL166
15BL168
15BL164
2000
1500
SW
c Lesponne
NE
500 m
and +
sill +
15BL179
15BL177
15BL176
sill +
and +
1500
1000

Figure 2

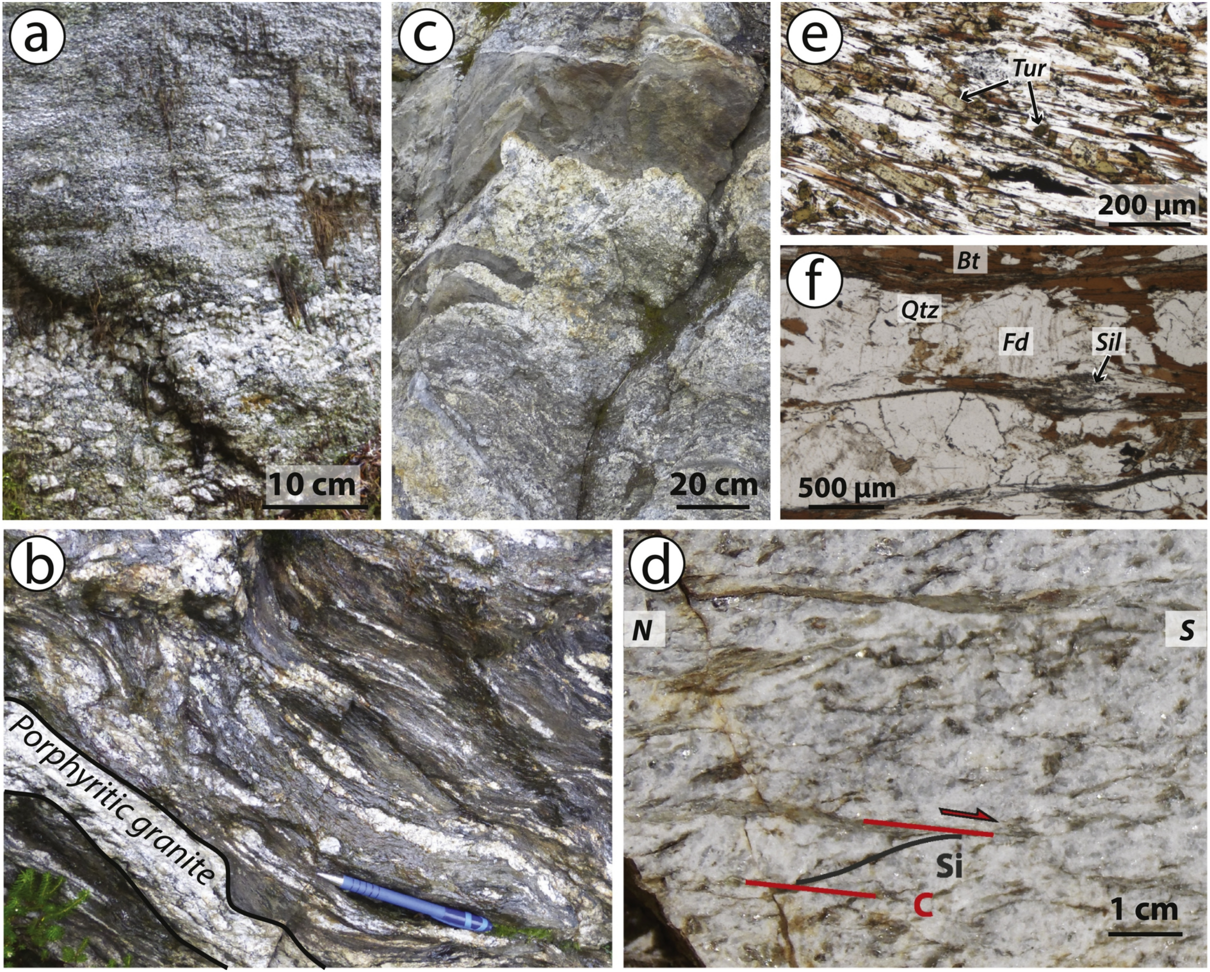
a
10 cm
b
Porphyritic granite
c
20 cm
d
N
S
Si
C
1 cm
e
Tur
200 µm
f
Bt
Qtz
Fd
Sil
500 µm

Figure 3

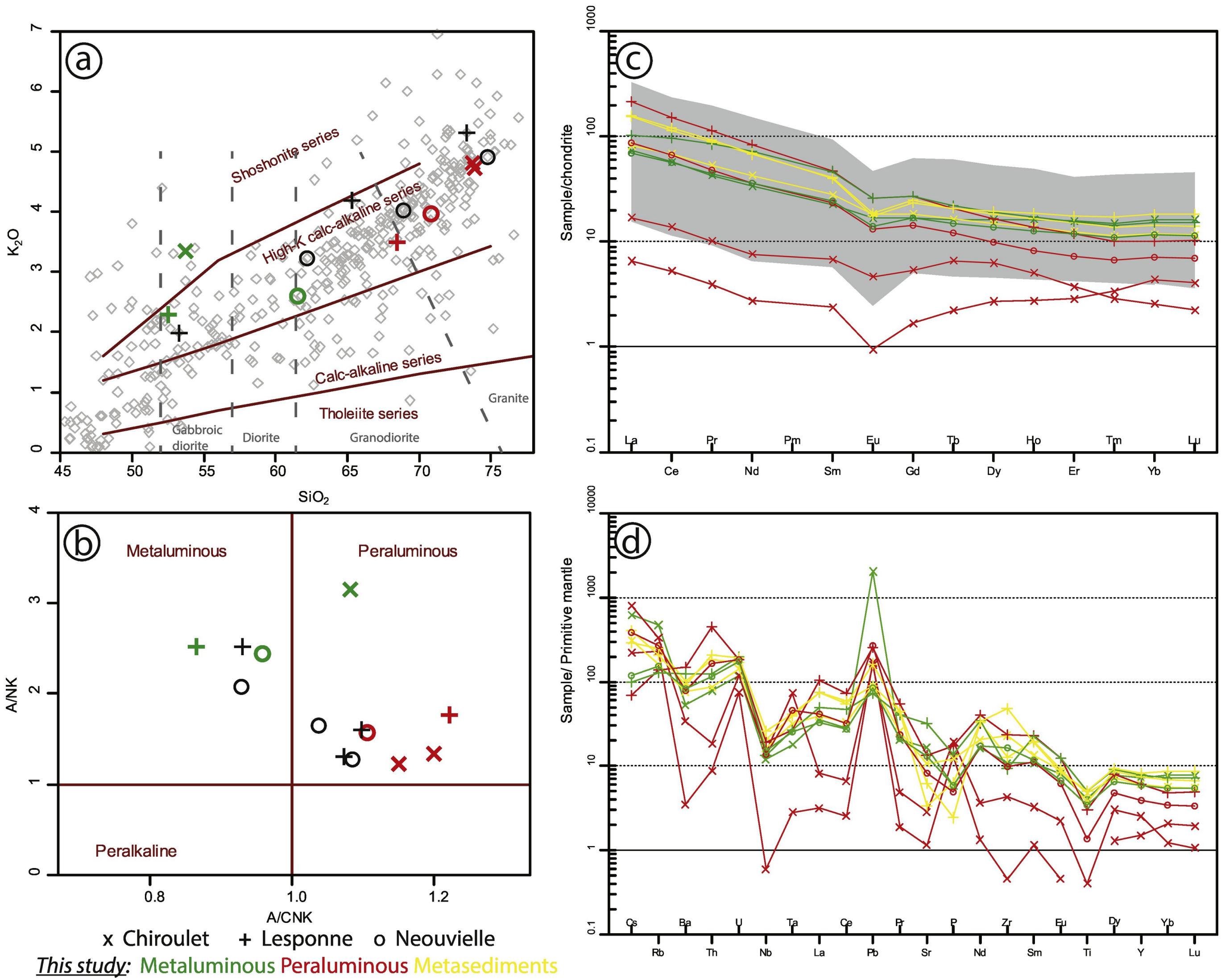
a
b
c
d
Shoshonite series
High-K calc-alkaline series
Calc-alkaline series
Tholeiite series
Gabbroic diorite
Diorite
Granodiorite
Granite
K2O
SiO2
Metaluminous
Peraluminous
Peralkaline
A/NK
A/CNK
Sample/chondrite
Sample/ Primitive mantle
x Chiroulet + Lesponne o Neouvielle
This study: Metaluminous Peraluminous Metasediments

Figure 4

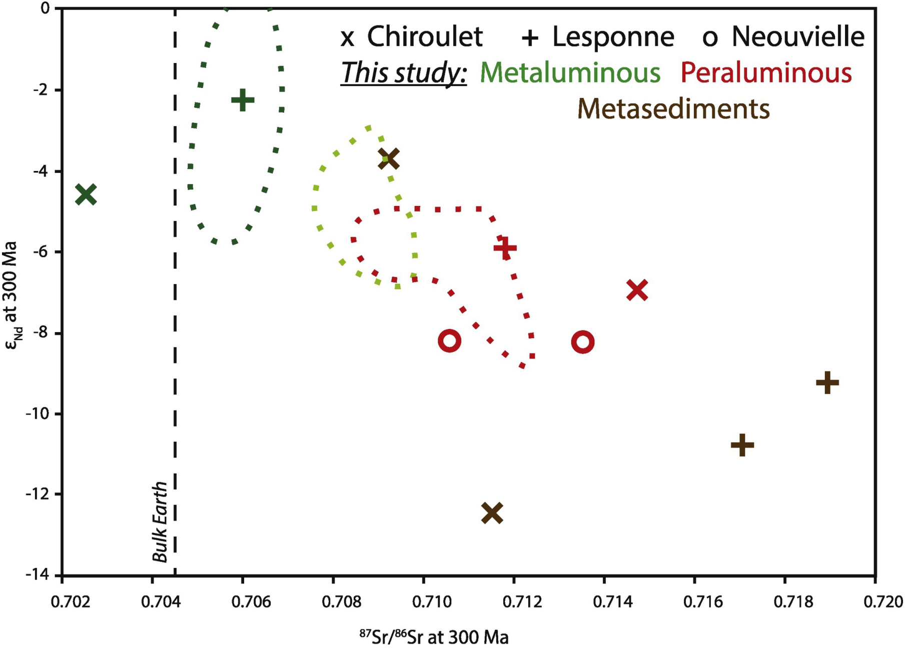
x Chiroulet + Lesponne o Neouvielle
This study: Metaluminous Peraluminous
Metasediments
Bulk Earth
ε_{Nd} at 300 Ma
0
-2
-4
-6
-8
-10
-12
-14
0.702
0.704
0.706
0.708
0.710
0.712
0.714
0.716
0.718
0.720
$^{87}Sr/^{86}Sr$ at 300 Ma

Figure 5

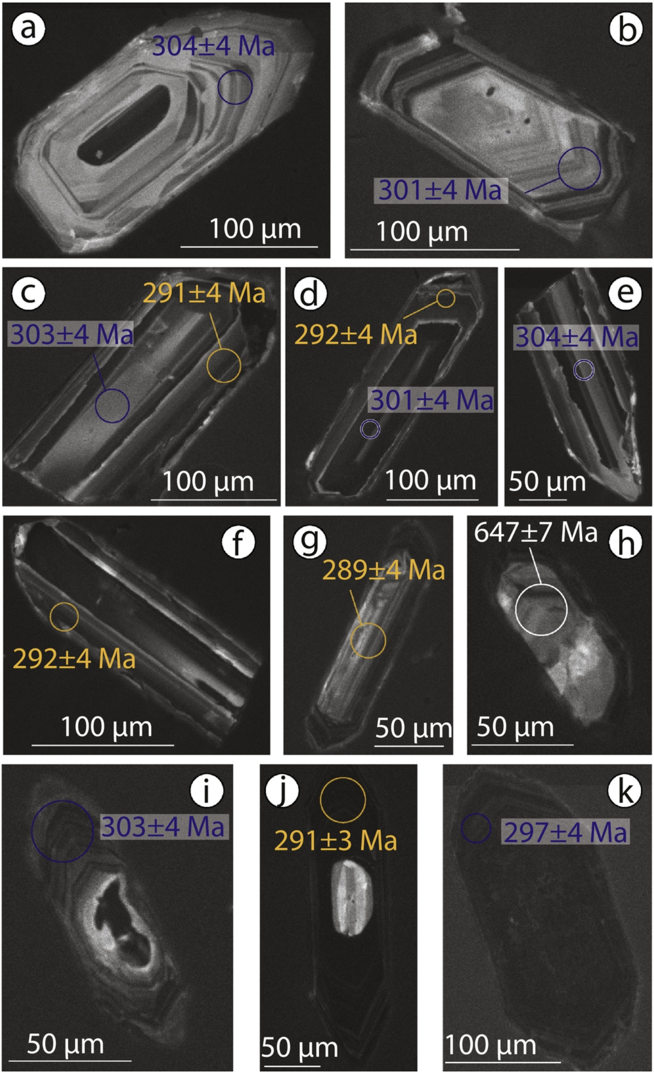
a
304±4 Ma
100 µm
b
301±4 Ma
100 µm
c
291±4 Ma
303±4 Ma
100 µm
d
292±4 Ma
301±4 Ma
100 µm
e
304±4 Ma
50 µm
f
292±4 Ma
100 µm
g
289±4 Ma
50 µm
647±7 Ma
h
50 µm
i
303±4 Ma
50 µm
j
291±3 Ma
50 µm
k
297±4 Ma
100 µm

Figure 6

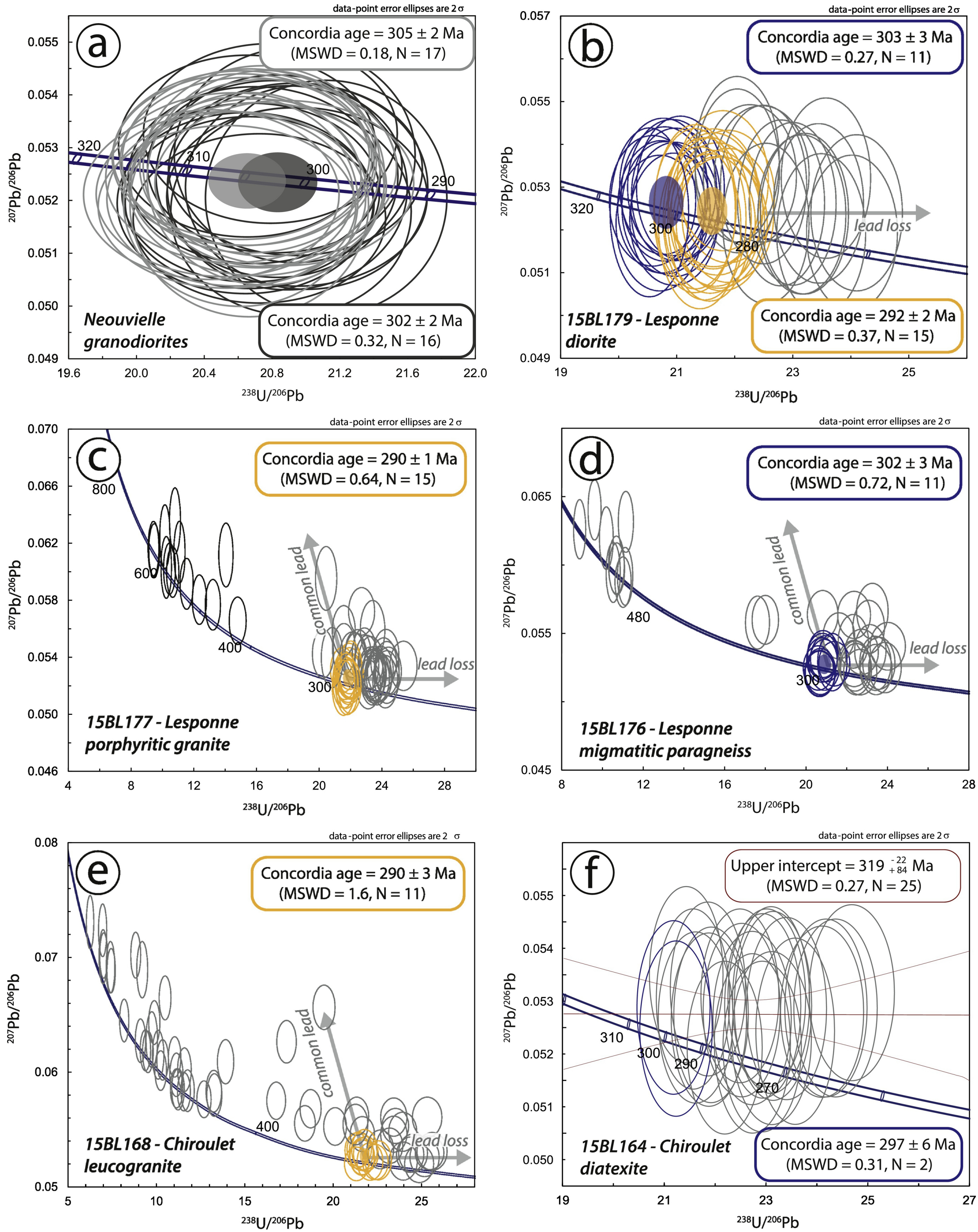
data-point error ellipses are 2 σ
a
Concordia age = 305 ± 2 Ma
(MSWD = 0.18, N = 17)
Concordia age = 302 ± 2 Ma
(MSWD = 0.32, N = 16)
Neouvielle granodiorites
320
310
300
290
$^{207}Pb/^{206}Pb$
$^{238}U/^{206}Pb$
b
Concordia age = 303 ± 3 Ma
(MSWD = 0.27, N = 11)
Concordia age = 292 ± 2 Ma
(MSWD = 0.37, N = 15)
15BL179 - Lesponne diorite
lead loss
320
300
280
c
Concordia age = 290 ± 1 Ma
(MSWD = 0.64, N = 15)
15BL177 - Lesponne porphyritic granite
common lead
lead loss
800
600
400
300
d
Concordia age = 302 ± 3 Ma
(MSWD = 0.72, N = 11)
15BL176 - Lesponne migmatitic paragneiss
common lead
lead loss
480
300
e
Concordia age = 290 ± 3 Ma
(MSWD = 1.6, N = 11)
15BL168 - Chiroulet leucogranite
common lead
lead loss
400
f
Upper intercept = 319 $^{-22}_{+84}$ Ma
(MSWD = 0.27, N = 25)
Concordia age = 297 ± 6 Ma
(MSWD = 0.31, N = 2)
15BL164 - Chiroulet diatexite
310
300
290
270

Figure 7

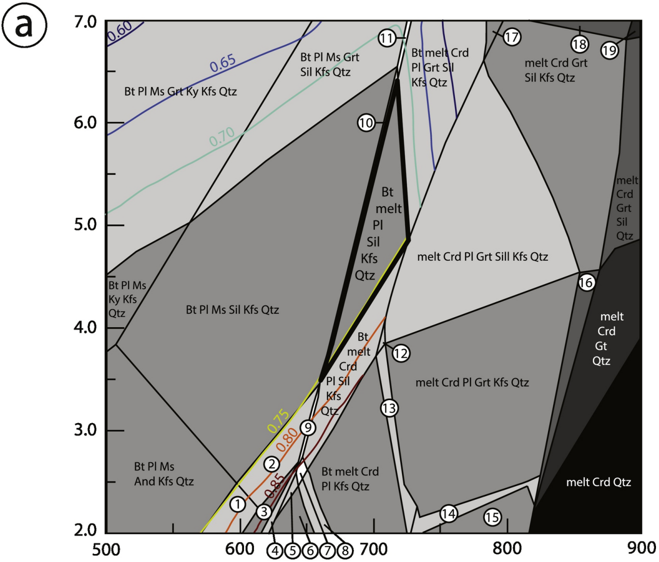

1- Bt Crd Pl Ms And Kfs Qtz; 2- Bt Crd Pl Ms Sil Kfs Qtz; 3- Bt Crd Pl Ms Kfs Qtz; 4- Bt Crd Pl Ms Kfs Qtz H_2O; 5- Bt Crd Pl Sil Kfs Qtz H_2O; 6- Bt Crd Pl Kfs Qtz H_2O; 7- Bt melt Crd Pl Sil Kfs Qtz H_2O; 8- Bt melt Crd Pl Kfs Qtz H_2O; 9- Bt melt Crd Pl Ms Sil Kfs Qtz; 10- Bt melt Pl Ms Sil Kfs Qtz; 11- Bt melt Pl Ms Grt Sill Kfs Qtz; 12- Bt melt Crd Pl Grt Sil Kfs Qtz; 13- Bt melt Crd Pl Grt Kfs Qtz; 14- Opx melt Crd Pl Grt Kfs Qtz; 15- Opx melt Crd Pl Kfs Qtz; 16- melt Crd Grt Qtz; 17- Bt melt Grt Sil Kfs Qtz; 18- melt Grt Sil Kfs Qtz; 19- melt Grt Sil Qtz

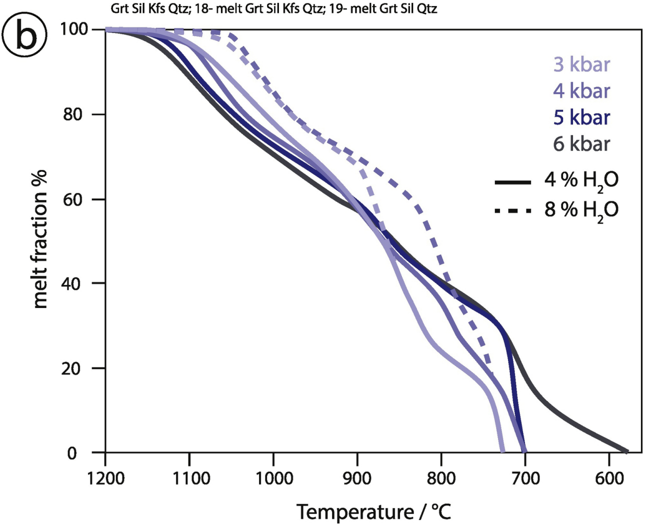

Figure 8

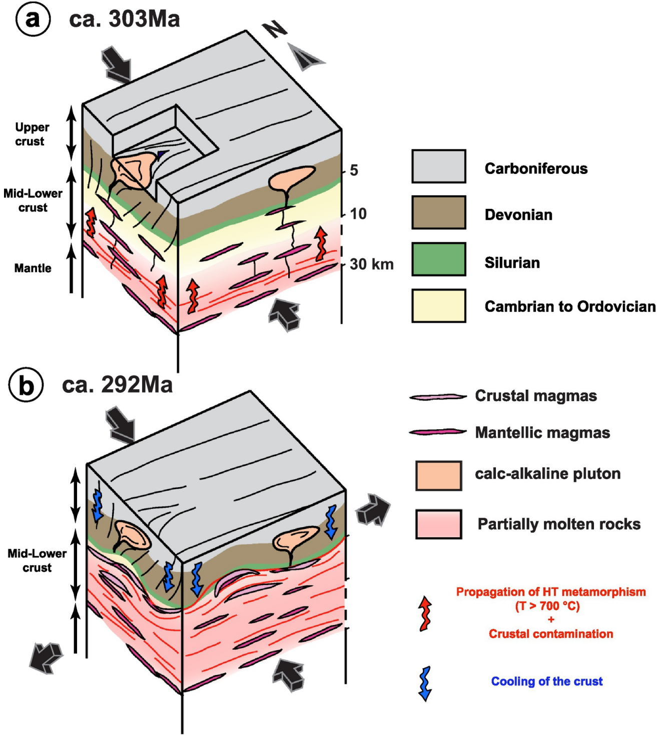
a
ca. 303Ma
N
Upper crust
Mid-Lower crust
Mantle
5
10
30 km
Carboniferous
Devonian
Silurian
Cambrian to Ordovician
b
ca. 292Ma
Mid-Lower crust
Crustal magmas
Mantellic magmas
calc-alkaline pluton
Partially molten rocks
Propagation of HT metamorphism
(T > 700 °C)
+
Crustal contamination
Cooling of the crust

Figure 9